COOLING OF NEUTRON STARS WITH QUARK CORE

by

Neilya Beisenkhanova

A thesis submitted in partial fulfillment
of the requirements for the degree

of

Master of Science

in

Physics

MONTANA STATE UNIVERSITY
Bozeman, Montana

February 2012

APPROVAL

of a thesis submitted by

Neilya Beisenkhanova

This thesis has been read by each member of the thesis committee and has been found to be satisfactory regarding content, English usage, format, citation, bibliographic style, and consistency and is ready for submission to The Graduate School.

Dr. Sachiko Tsuruta

Approved for the Department of Physics

Dr. Richard J. Smith

Approved for The Graduate School

Dr. Carl A. Fox

STATEMENT OF PERMISSION TO USE

In presenting this thesis in partial fulfillment of the requirements for a master's degree at Montana State University, I agree that the Library shall make it available to borrowers under rules of the Library.

If I have indicated my intention to copyright this thesis by including a copyright notice page, copying is allowable only for scholarly purposes, consistent with "fair use" as prescribed in the U.S. Copyright Law. Requests for permission for extended quotation from or reproduction of this thesis in whole or in parts may be granted only by the copyright holder.

Neilya Beisenkhanova

February 2012

DEDICATION

For my family.
Thank you for your love and for your encouragement. Without it my achievement would have seemed unattainable.

ACKNOWLEDGEMENTS

I would like to express sincere appreciation to the Physics Department at Montana State University (MSU) for their extended long-term support and especially to Professor Richard Smith for understanding and help I was provided through my study here.

I would specifically like to thank Dr. Sachiko Tsuruta, my advisor, whose personal and professional support, guidance and just simple care made this work possible. I would never been able to finish this without your support and care, Dr. Tsuruta. I also thank the members of my graduate committee for encouraging words and thoughtful criticism. My great acknowledgement to Dr. John Carlsten for fulfilling my knowledge of quantum mechanics in such a wonderful way of teaching and for a tremendous support and encouragement within all period of study. Thank you. Also, I would like to express my gratitude to Dr. Jiong Qiu for being in my graduate committee and just being such an understanding person.

I would like to thank the Bolashak International Scholarship of the President of the Republic of Kazakhstan for financial support and providing such an outstanding opportunity to study abroad. I acknowledge Mrs. Debora de Bode and Office of International Programs at MSU for mentoring, permanent assistance on different issues and just personal support through the whole period of study at MSU. A special thanks to Mrs. Margaret Jarrett and Mrs. Sarah Barutha, without whose knowledge and assistance with administrative issues this study would not have been successful. I really appreciate it.

TABLE OF CONTENTS

TABLE OF CONTENTS – CONTINUED

LIST OF TABLES

Table Page

LIST OF FIGURES

Figure Page

GLOSSARY

EoS – equation of state, the equation describing the state of matter under a given set of physical conditions, namely, pressure, density, temperature and composition.

URCA process – a set of nuclear reactions which emit neutrino and antineutrino in neutron star and white dwarf cooling processes. The name “URCA” was given by George Gamow and Mario Schoenberg and associated with “Casino da Urca” where, "the money disappeared at that roulette table as quickly as the energy disappears in the nucleus of the supernova”.

Direct URCA process – a set of nuclear reactions of beta decay and electron capture, which happens primarily in the neutron star core due to either high fraction of protons or due to the presence of “exotic” particles in the core.

Modified URCA process – a set of modified nuclear reactions of beta-decay and electron capture with spectator nucleons. One of the main processes responsible for neutron star cooling.

Hybrid stars – neutron stars with a mixed core, where hadrons can appear together with “exotic” particles, such as kaons, pions, hyperons and quarks.

“Best Buy” model – a most likely model.

ABSTRACT

Ordinary neutron stars can undergo two possible scenarios of cooling: with conventional `standard' neutrino emission processes or with faster `non-standard' processes. For both of these scenarios various mechanisms have been proposed. As possible nonstandard options, previous detailed studies already explored direct URCA processes involving hyperon-mixed matter and pion condensates. In the current research we explore another possible non-standard scenario - quark cooling where a hybrid star with a quark core undergoes direct URCA cooling. We used the exact evolutionary code originally constructed by Nomoto and Tsuruta (1987) which was modified for quark cooling. We chose a model with a medium equation of state TNI 6, where transition from neutron to quark matter takes place at a critical density of four times the nuclear density. Our results show that low mass stars undergo standard cooling while heavier stars, with mass larger than about $1.45M_{\odot}$, possess a central core where nonstandard accelerating quark cooling is in operation but it can be suppressed significantly due to density-dependent superfluid property. We showed that our quark cooling scenario can be consistent with the observational data on neutron star temperatures. An important result is that we obtained more realistic cooling behavior than obtained earlier, by adopting a density-dependent superfluid energy gap model, instead of constant gaps employed earlier.

CHAPTER ONE

INTRODUCTION

1.1 Historical Background

Since the beginning of 20th century the mechanism of stellar energy production has become gradually clear. One of the basic thermonuclear reactions in the Sun is hydrogen-helium conversion $4H \rightarrow He+\gamma+\nu$. This made astrophysicists to think: what would happen if the main fuel of stars, hydrogen, would exhaust? One possible end point of star's further evolution was a white dwarf which was discovered in 1914 by W.S. Adams (Adams W.S. Publications of the Astronomical Society of the Pacific). The first discovered white dwarf was about 1 solar mass with radius of about 20 000 km and average density of 10^7 g/cm^3.

For more massive stars the end of life is quite different. The stars which start out from 8 to 25 solar masses would end up with gravitational collapse during a Type II, Type Ib or Type Ic supernova event. In 1934, Baade and Zwicky, followed by discovery of neutrons in 1932 by Sir J. Chadwick, correctly proposed that the release of the gravitational binding energy of neutron stars powers these supernovae: "In the supernova process mass in bulk is annihilated" (Baade W., Zwicky F., 1934). If the central part of a massive star before its collapse contains (for example) 3 solar masses, then a neutron star of 2 solar masses can be formed. The binding energy E of such a neutron core, when expressed in mass units via the mass-energy equivalence formula $E = mc^2$, is about 1 solar mass. It is basically this energy that powers the supernova. During those years up to

1960s some pioneer theoretical calculations on neutron stars were carried out. In 1938 Oppenheimer and Volkoff calculated the structure of neutron stars, showing that a neutron star could have a central density as high as 10^{15} g/cm^3 when the mass of the neutron star is about 0.7 solar mass (Oppenheimer J.R., Volkoff G. M, 1939). Then a group of scientists, including Cameron, Hayakawa, Chiu and Salpeter (1959-1964) discussed various models of neutron stars and the equation of state. In 1964 S. Tsuruta was the first who carried out detailed calculations of thermal evolution of neutron stars due to neutrino and photon emission processes (Tsuruta S, 1964).

1.2 Detections of Neutron Star Temperatures

The first actual neutron star was discovered by Jocelyn Bell and Anthony Hewish quite by chance in 1968, when they received faint, but regular radio pulsating signals from the outer space (Hewish A., Bell S. J., 1968). Their proposal for the source of the signals was either white dwarfs or neutrons stars. The main feature J. Bell and A. Hewish accounted for was the extreme regularity of the pulses, with periods of 1.337s, which suggested them to be pulsation of the entire star as an origin rather than some disturbances in the stellar atmosphere. But according to the paper of Meltzer and Thorne, who calculated the periods for stars with certain densities (Meltzer, D. W., and Thorne, K. S., 1966), at a density of 10^7 g/cm^3, corresponding to a white dwarf star, the fundamental mode reaches a minimum period of 8s. Therefore for the periods of the order of 1s and less, the origin of these pulsations must be of very high densities of order 10^{13} g/cm^3 or higher, which corresponds to neutron stars.

Also neutron stars are not only being observed through radio telescopes, but in X-rays and Gamma rays too. In early 1960s unknown X-Ray sources were discovered by R Giacconi et al. (Giacconi et al., 1962) in the northern part of Scorpius, Sco X-1, which was soon followed by discovery of another X-ray source in Crab Supernova remnant (S. Bowyer et al., 1964). To explain these sources Chiu (Chiu H.Y., 1964) suggested such a source as a neutron star with surface temperature of about 10^7 K radiating as a blackbody. Due to the data from X-ray satellites such as UHURU, Einstein observatory and ROSAT, it is known now that many of the main energy source is a binary star system, where one member of this system is a neutron star. X-rays come from the accretion of materials from an ordinary star onto a neutron star.

The observational data obtained from the Einstein observatory helped the theorists to build thermal evolution theories of neutron stars. For example, the upper limits to the temperatures of neutron stars such as Crab, RCW 103 and 3C58 were consistent with so-called “standard” cooling scenario when the cooling mechanism involves conventional neutrino processes such as modified URCA, neutrino brehmsstrahlung and plasmon neutrino processes. However, for the Vela pulsar upper limit the predicted temperatures turned out to be too high, which implied that Vela neutron star would have cooled too fast for standard cooling. It was suggested then that the hotter stars can cool by the standard cooling scenario, while the cooler ones cool by non-standard cooling, such as pion or quark cooling, and the masses of the former class of stars should be somewhat less than those of latter (Tsuruta S., 1987).

The launch of the ROSAT X-ray satellite in 1990s confirmed for the first time the actual detection, not just upper limits, for stellar surface thermal radiation from at least three cooling stars: PSR (Pulsating Source of Radio) 0656+14, PSR 0630+18 (Geminga) and PSR 1055-52. The consequent detections by superior X-ray satellites helped to gain not only temperature upper limits, but also detections, as well as to estimate stellar composition, age and distances.

On the theoretical base calculations of neutron star cooling, such as EoS, superfluidity of constituent particles etc., have been carried out due to the important progress in nuclear, particle and quantum physics. These developments make it possible to construct better neutron star cooling models.

In this work we will consider a "best buy" model where some neutron stars with masses above $1.4M_{\odot}$ possess a mixed quark-hadronic central core (so-called hybrid stars), which undergoes non-standard accelerating cooling mechanisms. Magnetars, accreting neutron stars in binaries and millisecond pulsars are not included.

After an introduction in this chapter, we will discuss the basic equations for neutron star structure and evolution, major physical inputs and methods of solution in Chapter 2. In Chapter 3 we will discuss quark matter theory and summarize different models for neutron stars with quark core adopted by this theory. In Chapter 4 we present our theoretical model, discuss the results obtained for thermal evolution of a star with this model, and compare them with other latest theoretical research in this field. We conclude our work with the future prospect for research in hybrid star thermal evolution, and give our concluding remarks.

CHAPTER 2

STRUCTURE AND EVOLUTION OF NEUTRON STARS

2.1. Basic Equations

Stellar structure and evolution of stars are basically governed by three simple laws, namely hydrostatic equilibrium, energy balance and energy transport, and can be calculated via a series of relativistic differential equations involving mass, pressure, temperature, and density (Tsuruta S., 1998).

The basic equation of *hydrodynamic equilibrium* is given by the balance of the pressure gradient inside the star by the gravitational forces:

$$\frac{dP}{dr} = \frac{-G(m + 4\pi r^2 P / c^2)(P / c^2 + \rho)}{r^2 (1 - 2Gm / rc^2)} \tag{2.1}$$

Mass continuity equation:

$$\frac{dm}{dr} = 4\pi r^2 \rho \tag{2.2}$$

Gravitational potential due to general relativity:

$$\frac{d\varphi}{dr} = -\frac{dP/dr}{\rho c^2 + P} \tag{2.3}$$

Energy Balance:

$$\frac{dLe^{2\phi}}{dr} = -\frac{4\pi r^2 n e^{\phi} C_v dT / dt}{(1 - 2Gm / rc^2)^{1/2}} \tag{2.4}$$

and Radiative Energy Transport:

$$\frac{d(Te^{\phi})}{dr} = -\frac{-3k\rho L_{\gamma} e^{\phi}}{16\sigma T^3 4\pi r^2 (1 - 2GM / rc^2)} \tag{2.5}$$

where r is the radial distance from the stellar center, m(r) is the mass inside radius r, ρ(r) is energy density, P(r) is total pressure, T is temperature, L is total luminosity, Lγ is total photon luminosity (energy transported by photons in the units of Joule per second), φ(r) is the gravitational potential, n is total number density, C_v is total specific heat, κ is total opacity, and e^{φ} is the general relativistic correction factor. G, σ and c are gravitational constant, Stefan-Boltzmann constant, and speed of light, respectively. In the non-relativistic limit these equations reduce to the familiar Newtonian stellar structure equations, where e^{φ} reduces to 1, $m \square 4\pi r^3 P$, and $P \square \rho c^2$.

The first equation (2.1) describes a force balance between gravity and internal pressure gradient. The second one (2.2) is a known relation between mass and density. The third equation (2.3) defines gravitational potential due to general relativity which becomes relevant in neutron star structure, as soon as its radius is about 10 km (about 3 times the Schwarzschild radius). These three equations determine the structure and mechanical properties of the star such as the relations between mass, radius and central density.

The last two equations determine the thermodynamic properties of the star, such as specific heat, luminosity and internal and surface temperatures.

Equation (2.4) is especially important to describe the cooling processes in neutron stars. In the Newtonian limit the equation will reduce to the following:

$$\frac{dE}{dt} = -C_v \frac{dT}{dt} = L_\gamma + L_v - H \tag{2.6}$$

where E is the total internal energy, L_γ is photon luminosity, L_υ is neutrino luminosity, C_v is total specific heat and H is heating rate when heating becomes important. Equation (2.6) represents the cooling rate with time which will be discussed in 2.2.1.

To solve these equations we need additional supplementary equations such as:

Equation of State (EoS):

$$P = P(X, \rho, T) \tag{2.7}$$

See Appendix A for the detailed expression of EoS.

Opacity Equation:

$$\frac{1}{k} = \frac{1}{k_R} + \frac{1}{k_c} \tag{2.8}$$

where κ is total opacity, κ_R is radiative transfer opacity and κ_c is opacity due to heat conductivity.

Luminosity Equations:

$$\frac{dL_v e^{2\phi}}{dr} = \frac{4\pi r^2 n e^{\phi} \varepsilon_v}{(1 - 2Gm/rc^2)^{1/2}} \tag{2.9}$$

$$L_\gamma = 4\pi\sigma R^2 T_s^4 \tag{2.10}$$

$$L = L_\gamma + L_v \tag{2.11}$$

where L is total luminosity, L_γ is photon luminosity, L_v is neutrino luminosity, ε_v is neutrino emissivity and n is total number density.

Here we should take into account the gravitational effects on temperature T, photon luminosity L_γ, and radius R due to the high densities of neutron star. These values will be gravitationally redshifted at infinity, so the corrections are:

$$T_s^\infty = T_s e^{\varphi_s} \tag{2.12}$$

$$L_s^{\infty} = L_{\gamma} e^{2\varphi_s} \tag{2.13}$$

$$R_e = R e^{-\varphi_s} \tag{2.14}$$

where R_e is an effective (observed) radius, φ_s is the gravitational potential at the stellar surface, and

$$e^{\varphi_s} = (1 - 2Gm / rc^2)^{1/2} \tag{2.15}$$

Putting these equations together, we will get an expression for the observed photon luminosity:

$$L_{\gamma}^{\infty} = 4\pi\sigma R_e^2 (T_s^{\infty})^4 \tag{2.16}$$

2.2 Methods of Solution

2.2.1 Exact Evolutionary Method

Solving equations (1) to (10) simultaneously we will obtain the mechanical and thermodynamic properties of the star such as mass M, radius R, central density ρ_c, temperature T, total internal energy E, specific heat C_{υ}, as well as the radial distribution of all of these parameters inside the stellar interior. This method of solution is called the "exact evolutionary method".

Typical cooling curves obtained by the exact evolutionary method are shown in figure 2.1, where photon luminosity L_{γ} is plotted vs. stellar age *t*. The different curves refer to different EoS such as BPS or soft (Baym, Pethick and Sutherland, 1971), PS or stiff (Pandharipande, Pines, Smith, 1976), and FP medium (Friedman, Pandharipande, 1981) models. The data points are indicated by the name of observed pulsars, bars and downward arrows represent detections and upper limits, respectively. During the first 10^5

years the star cools by neutrinos escaping from the interior and this period is called the *neutrino cooling era*. Later photon luminosity dominates during the *photon cooling era*.

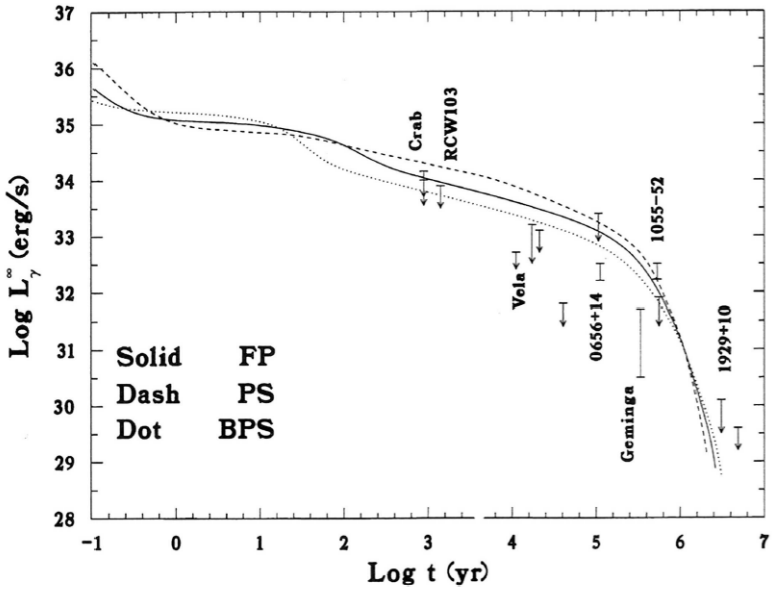

Figure 2.1. Typical standard cooling curves for different neutron star models BPS (dotted curve), PS (dashed), and FP (solid) (S. Tsuruta, 1998).

At high temperatures neutrino luminosity exceeds photon luminosity, but then it has a sharp decrease as luminosity depends on core temperature as $L_\upsilon \propto T^{6\text{-}8}K$, while photon luminosity depends on the temperature more moderately as $L_\gamma \propto T^4K$. This is shown in figure 2.2, where the three steeper slopes refer to modified URCA, plasmon and crust bremsstrahlung neutrino luminosity and the two softer slopes are referred to photon luminosity.

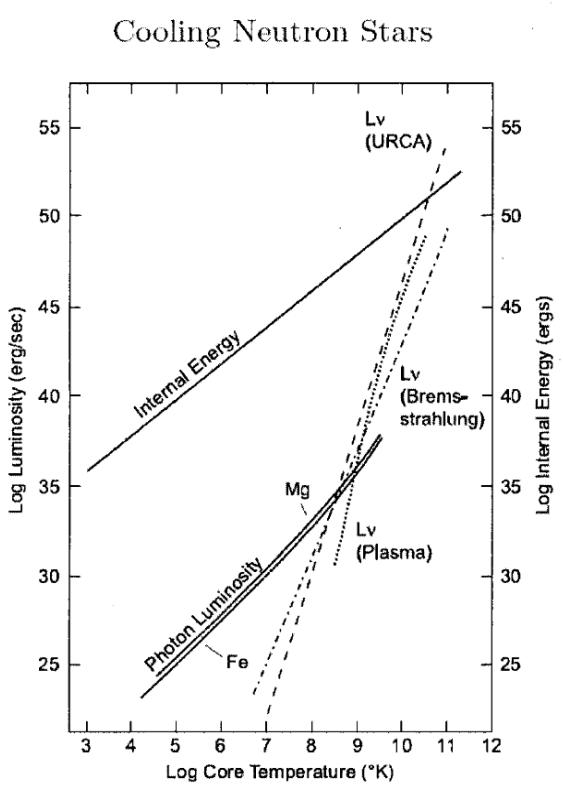

Figure 2.2. Various neutrino and photon luminosities and internal energy are shown as a function of the internal core temperature (Tsuruta S., Cameron A., 1966).

2.2.2 Isothermal Method

According to the isothermal method we can decouple the mechanical and thermodynamic equations (2.1) – (2.5). The neutron star interior is assumed to be isothermal and any change to the temperature occurs only within the thin outer layers, called an envelope, near to the surface. Decoupling and integrating separately equations (2.1) to (2.3), from stellar center to surface, we obtain the mechanical properties such as M, R and ρ_c. Using these quantities as an input we solve the equations (2.4) and (2.5) to obtain thermodynamic properties such as the relation of temperature vs. time, e.g. cooling processes, and the relation between core temperature T_c and surface temperature T_s. The

latter relation is crucial as photon and neutrino luminosities depend on the surface and core temperatures, respectively.

2.3 Major Physical Input

In this section I consider the most important factors that may affect the processes in neutron stars. They are: composition, EoS (equation of state), neutrino emissivity, superfluidity of constituent particles, total opacity, and effect of heating.

2.3.1 Composition and Structure

The gravitational field at the surface of a neutron star is extremely large. For a solar mass star of radius 10 km the gravitational binding energy at the surface of the star is ~ 100MeV per atomic unit, which means an electron would be bound gravitationally to the star a thousand times more strongly than in hydrogen atom nucleus. As the matter is compressed the electron Fermi energy rises and the electrons break free from their nuclei. At densities of $\sim 10^6 g/cm^3$ all the electrons are free and relativistic and the electron Fermi pressure reaches the point where it can support the interior of the star, namely a white dwarf, against gravitational collapse.

2.3.1.1 Outer Crust ($\rho < 4.3\times10^{11} g/cm^3$) Near the surface, the spacing between nuclei r_0 is larger than the nucleus size R_N,

$$r_0 \sim 2/3\ 10^5\ \rho^{-1/3} R_N \qquad (2.17)$$

and the Coulomb interaction between the nuclei is not sufficient for provoking beta decay of stable nuclei. Hence the nuclear species that we expect are those of main sequence

fusion elements, i.e. dominantly iron group elements. To determine whether the surface is solid or plasma we would need to know if the energy for lattice formation is less than Coulomb energy. The criterion of $r_0 >> 14/AZ^2 \times 10^{-13}$cm would be for a solid crust around the neutron star (Irvine J.M., 1975).

As the density increases there are more and more neutron-rich nuclei. This happens in the electron capture process, when free electrons are captured by protons in nuclei due to the high densities (of $\sim 10^9$g/cm^3 and higher) and become neutrons within the nucleus.

2.3.1.2 Inner Crust (4.3×10^{11}g/cm^3< ρ<2.8×10^{14}g/cm^3). Near the densities of 4.3×10^{11}g/cm^3 and higher, free neutrons will drip out from nuclei. We call these densities "neutron-drip" densities; in this region, free neutrons, free electrons and neutron-rich heavy nuclei exist together. When the densities reach the so-called nuclear density of $\rho_0 = 2.8\times10^{14}$g/cm^3, the nuclei start to disintegrate into neutron dominated matter and the matter consists of primarily neutrons with a small fraction of protons and electrons.

2.3.1.3 Core ($\rho>2.8\times10^{14}$g/cm^3). When the density is not high enough the composition of the central core is predominantly neutrons (95%). This occurs in the region where $\rho_0<\rho<\rho_{tr}$, where ρ_{tr} is a transition density to exotic particles, such as hyperons, pions, and quarks. When a neutron star is less massive and therefore less dense it is considered to be ordinary neutron matter. For higher densities the exotic particles would appear. So, for the more dense and massive star the inner core is a mix of exotic particles and the outer core is the neutron matter.

2.3.2 Equation of State

The equation of state is one of the crucial inputs for neutron star matter calculations. Under the standard conditions the matter is strongly degenerate and the pressure of the matter is temperature independent. When the densities reach the point of $\sim 10^8 g/cm^3$ the EoS is not affected by even very strong magnetic fields (of $\sim 10^9 G$) and temperatures ($>10^7 K$).

An equation of state for neutron matter depends on the nuclear force between nucleons and for exotic particle matter depends on the strong interaction. The behavior of the nuclear force is illustrated on Figure 2.3 where the nuclear potential V is plotted via the separation distance.

According to Figure 2.3 the nuclear force is generally negative and become attractive at first when the distances decrease, but then it turns to positive and therefore repulsive as the distances become small enough.

The relationship between attractive and repulsive effects of the nuclear potential determines the EoS of the core. Model A in Figure 2.3 has stronger attractive force and therefore it is related to a denser, more compact and smaller star. The EoS of such a model is called “soft”. For Model B the repulsive force is stronger and it will result in a less dense, more extended and larger star.

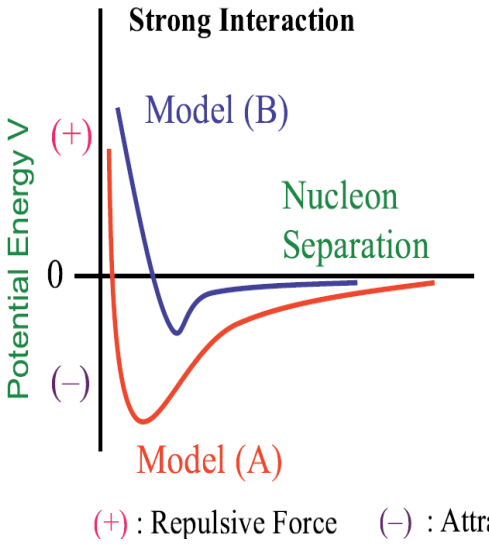

Model	(A)	(B)
ρ^c (gm/cm^3) /10^{14}	3 ~ 70	3 ~ 10
Mass/$M_\odot$	0.1~1.5	0.1 ~ 2
Radius (km)	20 ~ 8	20 ~15

Properties of NS - Model dependent!

Figure 2.3. Nuclear force: Simplified representation of the nuclear potential shown as a function of the separation between two nucleons (Tsuruta S., 2010).

The EoS for this kind of model is called “stiff”. Table 2.1 represents the pressure vs. density relation for representative soft, stiff and medium EoS.

Table 2.1 Pressure vs. density relation for different EoS.

Log (ρ)	Log (P)		
	Model FP (medium)	Model PS (stiff)	Model BPS (soft)
11.02	29.17468	29.17465	29.17468
11.32	29.5172	29.51716	29.5172
11.63	29.89241	29.89237	29.89241
11.93	30.04269	30.04265	30.04269
12.15	30.21929	30.21925	30.21929
12.43	30.42488	30.42484	30.42488

Table 2.1 Continued. Pressure vs. density relation for different EoS.

12.65	30.6263	30.62626	30.6263
13.2	31.36316	31.36312	31.43889
13.42	31.69965	31.69961	31.76297
13.69	32.12194	32.1219	32.17
13.91	32.46582	32.80718	32.55143
14.24	33.08502	33.62062	33.1472
14.46	33.65866	34.15431	33.56186
14.7	34.2917	34.76411	34.07811
14.8	34.56619	35.01718	34.40704
15	35.1392		34.80771
15.32	36.17873		35.79082
15.58	36.93885		36.4637
15.72			36.4637

2.3.3 Neutrino Emissivity

About 20 s after its birth, a neutron star becomes transparent to neutrinos generated in its interior. The neutrinos carry away the thermal energy of neutron stars and the star cools. Therefore, a study of neutrino reactions is important for NS cooling theories.

2.3.3.1 Neutrinos. The electron neutrino was first postulated in 1930 by Wolfgang Pauli to explain why the electrons in beta decay were not emitted with the full reaction energy of the nuclear transition. The conservation of energy dictated for the beta-decay reaction gives electron energy (Griffiths D., 1987):

$$E = \left(\frac{m_A^2 - m_B^2 + m_e^2}{2m_A} \right) c^2 \tag{2.18}$$

where, m_A is the mass of radioactive nucleus, m_B is the mass of lighter daughter nucleus and m_e is mass of an electron. The value of E should be fixed while the experiments showed that the electrons varied considerably in energy. This fact brought the scientists to the thought that either the energy conservation law was violated or there must be another particle which was emitted along with the electron which carried the "missing" energy. It was proposed that the new particle was a neutrino (called so, due to the extremely small mass) and the fundamental beta-decay process now is known as:

$$n \rightarrow p^+ + e^- + \overline{\nu_e} \tag{2.19}$$

where $\overline{\nu_e}$ is antineutrino, which differs from neutrino by lepton number L (which is +1 for the neutrino and -1 for the antineutrino).

Neutrinos are a subject for weak interactions with other particles due to their low mass and neutral charge. This feature of neutrinos helps scientists to use them as a probe for environments, such as supernovae, where any other particles cannot penetrate. The core of a collapse event of a supernova is very dense and highly energetic, so no known particles can escape the core front other than neutrinos. Supernovae are known to release approximately 99% of their radiant energy in a short (twenty second) burst of neutrinos.

During the early "neutrino era" neutron stars cool predominantly due to neutrinos escaping directly from the interior. The effective mean free path of neutrinos:

$$\lambda = (\sigma n)^{-1} = (\sigma_n n_n)^{-1}(\sigma_c n_c)^{-1} = 2\times10^{15}\text{km}\ (\rho_o/\rho)^{7/6} \times 100\text{keV}/(E_\upsilon)^{5/2} \sim 200\text{km} \qquad (2.20)$$

where n_n and n_c are the neutral and charged particle number densities and σ_n and σ_c are the neutral and charged particle cross sections, respectively. The effective mean free path is about ~ 100 km which is much longer than the radius of the neutron star ~ 10 km. So the neutrinos pass and escape the stars unimpeded (Qin L., 1995).

Neutrino emissivity, ε_ν, can be divided into two parts: emissivity for slower, more conventional "standard" processes ε_ν (st) and emissivity for fast "non-standard" processes ε_ν (nonst):

$$\varepsilon_\nu = \varepsilon_\nu\ (\text{st}) + \varepsilon_\nu\ (\text{nonst}) \qquad (2.21)$$

ε_ν (st) can be expressed as:

$$\varepsilon_\nu\ (\text{st}) = \varepsilon_\nu^{MU} + \varepsilon_\nu^{NN} + \varepsilon_\nu^{pl} + \varepsilon_\nu^{B}(C) + \varepsilon_\nu^{(\text{others})} \qquad (2.22)$$

where ε_ν^{MU}, ε_ν^{NN}, ε_ν^{pl}, $\varepsilon_\nu^{B}(C)$ are modified URCA, nucleon bremsstrahlung (involving both neutrons and protons), plasmon and crust bremsstrahlung neutrino emissivity, respectively.

Inside the core, the basic processes are the modified URCA and nucleon bremsstrahlung processes. Inside the crust, the major processes are the electron-ion modified URCA, neutrino bremsstrahlung process and the direct coupled electron-neutrino processes, such as plasmon-neutrino, photon-neutrino and electron positron pair neutrino processes.

2.3.3.2 Modified URCA Processes. These processes have been treated as the main neutrino generation mechanism for standard neutron star cooling according to Chiu H. and Salpeter E. (1968).

The modified URCA reaction is similar to the familiar reactions of beta decay and beta capture, but involves an additional nucleon. The modified URCA process proceeds as follows:

$$n + n \rightarrow n + p + e^- + \bar{\nu}_e \quad (2.23)$$

$$n + p + e^- \rightarrow n + n + \nu_e \quad (2.24)$$

The spectator nucleon is needed to conserve the momentum of reacting particles. The familiar beta-decay and beta-capture reactions (called the direct URCA process discussed below) are forbidden in the outer neutron star core. The suppression is due to the relatively low fractions of electrons and protons, according to which the Fermi momenta of n, p, and e do not obey the `triangle rule':

$$p_{Fn} \leq p_{Fe} + p_{Fp}, \quad (2.25)$$

required for momentum conservation.

Modified URCA process involving heavy ions takes place in the crust also.

2.3.3.3 Neutrino Bremsstrahlung Due to Nucleon-Nucleon Scattering. The n-n and n-p bremsstrahlung processes are:

$$n + n \rightarrow n + n + \nu + \bar{\nu} \quad (2.26)$$

$$n + p \rightarrow n + n + \nu + \bar{\nu} \quad (2.27)$$

Nucleon neutrino bremsstrahlung takes place in the core, while crust neutrino bremsstrahlung takes place in the inner crust. In the crust the electron-ion neutrino bremsstrahlung is due to the collisions between electron and nuclei:

$$e^- + (Z,A) \rightarrow e^- + (Z,A) + \nu_e + \bar{\nu}_e \quad (2.28)$$

Here, the kinetic energy of the participating particles is transformed into neutrino-antineutrino pairs.

$\varepsilon^{(others)}$ represents other minor standard neutrino emissivity processes such as pair neutrino, photo-neutrino processes etc.

These processes are called "standard" because the mechanisms were straightforwardly predicted and have been adopted since early 1960s.

It was shown first in 1965 by Bahcall J. and Wolf R. (1965) that the cooling processes in the neutron stars may go much faster due to the presence of the "exotic" particle condensates in the core. Moreover, it has been shown that if the proton fraction in neutron matter is ~11% or more a fast direct URCA process involving nucleons alone (without exotic particles) also can take place in the neutron-dominated core (Lattimer J. et al., 1991).

2.3.3.4 Direct URCA Process. The sequence of beta-decay and beta-capture reactions

$$n \rightarrow p + e + \bar{\nu} \quad (2.29)$$

$$p + e \rightarrow n + \bar{\nu} \quad (2.30)$$

called the direct URCA process, is forbidden in the outer neutron star core due to insufficiently high fractions of e and p. It had been thought for a long time that the process is also forbidden in the inner neutron star core.

However, the processes (2.29)-(2.30) become allowed (Lattimer J.M., Pethick C.J., Prakash M, Haensel, 1991), if the fraction of protons (among all baryons) $x_p = n_p/n_b$ exceeds some critical value $x_p = x_c$. It was the paper by Lattimer et al. (1991) where it was shown that, for some realistic models of matter, x_p slightly exceeded x_c at densities several times higher than the standard nuclear matter density. Therefore, the nucleon direct URCA process can be allowed in the inner cores of rather massive neutron stars. The direct URCA process takes place in hyperon, pion, kaon and quark matter also. The neutrino emissivity in the direct URCA process is about 5-6 orders of magnitude more efficient than the modified URCA. Therefore, sufficiently massive neutron stars suffer enhanced cooling.

2.3.3.5 Neutrino Emission Due to Cooper Pairing of Nucleons. The onset of nucleon superfluidity switches on a new neutrino generation mechanism concerned with the creation of Cooper pairs. The process had been proposed and calculated in the pioneering article by Flowers E. et al. (1976). It was Page D. et al (2004) who introduced the process into the cooling theory. The process represents neutrino pair emission (any neutrino flavor) by a nucleon N (neutron or proton) whose dispersion relation contains an energy gap:

$$N \rightarrow N + \nu + \bar{\nu} \qquad (2.31)$$

The reaction cannot occur without superfluidity: the emission of a neutrino pair by a free nucleon is forbidden by energy - momentum conservation.

The efficiency of the process can be comparable to or even larger than the efficiency of the modified or even the direct URCA processes suppressed partly by the superfluidity. This determines the importance of `Cooper' neutrinos for neutron star cooling. Neutrino emission due to pairing of protons appears to be much weaker owing to the smallness of the vector constant of the weak neutral current involving protons.

In Figure 2.4 standard and non-standard cooling curves are shown for a 1.4 $M_{\odot}$ star.

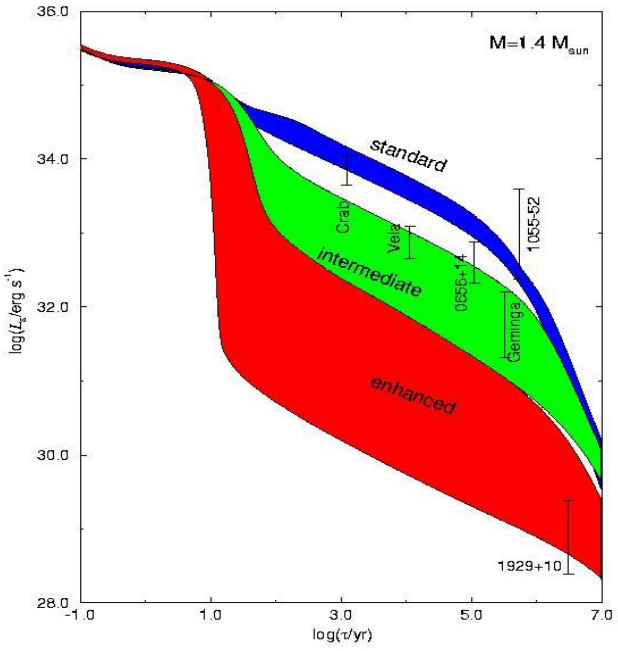

Figure 2.4. Standard and non-standard cooling curves for a 1.4 $M_{\odot}$ star.

2.3.4 Superfluidity of Constituent Particles

As the central collapsed star cools after a supernova explosion and the interior temperature falls below the superfluid critical temperature T_{cr}, the constituent particles (nucleons, hyperons, pion condensates, quarks, but not electrons and muons) become superfluid. In 1958 Bohr A., Mottelson B. and Pines D. (Bohr et al., 1958) suggested that this phenomenon much like superconductivity of electrons could appear in systems of nucleons in atomic nuclei. Cooper pairing of nucleons could occur due to nuclear attraction. It was expected that the gap in the nucleon spectrum, $\Delta \sim 1$ MeV ($T_c = 10^{10}$ K), was many orders of magnitude larger than for electrons in metals. Migdal A. (1971) was one of the first who applied the superconductivity theory to atomic nuclei. He noticed also that neutron superfluidity caused by nuclear forces could occur in neutron matter where critical temperatures of $T_{cr} = 10^{10}$ K could be expected. At lower densities (with total density at $\sim 10^{13\text{-}14}$g/cm^3) neutrons in the inner crust are expected to be in the $^1S_0$, when the temperature decreases below critical temperature T_{cr}. In this case, the energy gap is isotropic, independent of the orientation of nucleon momentum.

When total density is $\sim 10^{14\text{-}15}$g/cm^3 superfluid neutrons in the core are expected to be in a triplet state $^3P_2$, respectively, while protons in the core are in the $^1S_0$ state, as the partial densities of protons are $\rho < 10^{14\text{-}15}$g/cm^3. Hereafter, we refer to neutron superfluid in the $^1S_0$ state in the crust as "neutron S", and neutron superfluid in the $^3P_2$ state in the core as "neutron P" superfluid.

A very important contribution to the theory was made in the paper by Hoffberg et al. published in 1970. The authors showed that the triplet-state $^3P_2$ interaction of neutrons

at $\rho>\rho_0$ is attractive. Thus, triplet-state neutron superfluidity with an anisotropic gap can occur in the NS core. The authors performed the first calculations of the critical temperature of the triplet-state neutron superfluidity in NSs.

In the superfluid state, the thermodynamic properties of baryons decrease as a function of T_{cr}/T. The superfluid critical temperature T_{cr} is related to the superfluid energy gap Δ according to:

$$k\,T_{cr} = 0.57\Delta \qquad (2.32)$$

where k is Boltzmann constant and Δ represents strength of superfluidity.

For the core neutron superfluidity, the gap energy and the corresponding critical temperature are strongly model dependent. First, if a nuclear potential model which gives a stronger attractive force is used, the energy gap becomes larger. The second factor which is more important is the neutron effective mass m_n^*. Generally, the gap energy decreases as m_n^* decreases. In the first estimation of the neutron P superfluid energy gap made by Hoffberg M. et al. (1970), called HGRR model, with $m^*=1$, the resulting energy gap (and hence critical temperature) extends to high density regions. Here $m^* = m_n^*/m_n$, where m_n is neutron mass. In some other core neutron superfluid models, e.g. Takatsuka T. (1972) or T72 model and by Amundsen L. and Østgarrd E. (1985), AO model hereafter, density dependent m^* is used. For illustration, we present the critical temperature of the triplet-state neutron superfluidity obtained by different authors in Fig. 2.5.

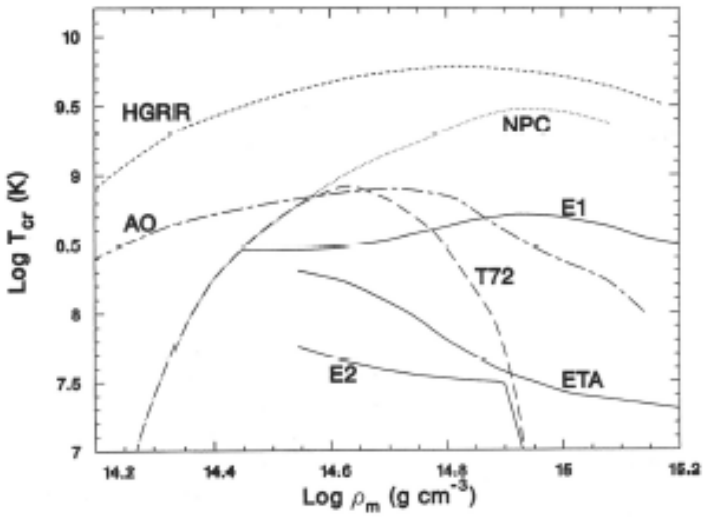

Figure 2.5. Density dependence of T_{cr} for various core neutron P superfluid models (Tsuruta S., 1998).

The HGRR curve has been calculated by Hoffberg et al. (1970) for neutron superfluidity using the nucleon-nucleon potential which reproduces quite well experimental phases of nucleon scattering at energies 4 320 keV. The in-medium effects have been neglected; the effective neutron mass has been set equal to its bare mass. The TT-curve has been calculated by Takatsuka T. and Tamagaki R. (1972) for the neutron superfluidity under the same assumptions but using the one-pion-exchange model of nucleon interaction (OPEG ^{3}O-1) with a somewhat harder core. This lowers T_{cr}. The solid AO-curve was obtained by Amundsen M. and Ostgaard E. (1985) for neutron superfluidity using a similar one-pion-exchange approach (OPEG), but the effective neutron mass was determined self-consistently and appeared to be lower than the bare neutron mass. NPC, ETA, E_1 and E_2 models were constructed by Takatsuka T. and Tamagaki R. in 1980-1982.

The major effect of superfluidity on cooling is that when the interior temperature T becomes below T_{cr}, all neutrino processes involving the superfluid particles decrease roughly as:

$$L_\nu \text{ (super)} = L\nu \text{ (normal) } R\ (T/T_{cr}) \qquad (2.33)$$

where L_ν(super) and L_ν(normal) are neutrino luminosities with and without superfluid particles, respectively, and $R(T/T_{cr})$ is a reduction factor. In the presence of superfluidity a star cools more slowly due to suppression of neutrino cooling, which raises surface temperature during the neutrino cooling era. The suppression is larger for stronger superfluidity, which means that for a larger energy gap the T_{cr} is higher. This effect on cooling is small for crust neutrons, but it can be significant for core particles.

Thus, the effect of superfluidity on cooling curves would result in raising the temperature curves during the neutrino cooling era. This effect might be drastic for non-standard cooling. Figure 2.6 shows the cooling curves for $1.4M_\odot$ star with FP (medium) EoS for different T_{cr}. Different models HGRR, T72, AO etc., refer to the superfluid models introduced in Figure 2.5. For a weak superfluid model such as Model T72 the superfluid suppression is very small, but for a strong model, such as HGRR, the superfluidity effect is so high, that the cooling process goes through the standard scenario.

We see that the effect of superfluid core neutrons is to raise the surface temperature during the neutrino cooling era. Proton superfluidity also gives similar effects. Another important factor is that superfluidity causes additional neutrino processes, hereafter

referred to as the 'Cooper pairing neutrino processes', which were suggested by Flowers et.al in 1976 and rediscovered by Yakovlev et.al in 1999.

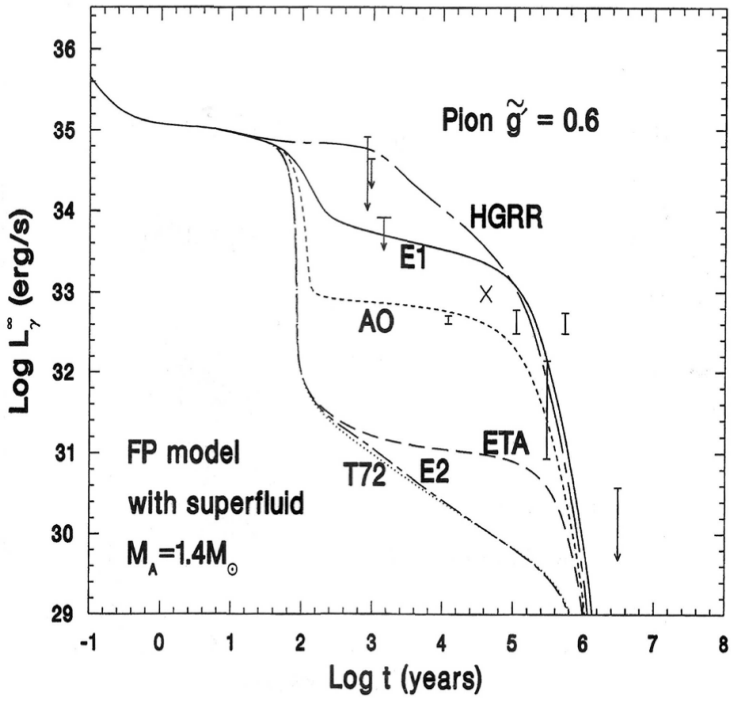

Figure 2.6. The effect of superfluidity on non-standard cooling (Tsuruta S., 1998).

The net effect is to enhance the neutrino emission involving the superfluid particles right after the superfluidity sets in. The effect is especially important when core neutrons are in a superfluid state.

2.3.5 Opacity

Inside neutron stars, there are two ways to transfer energy from the interior to the surface: radiation and conduction. The energy transfer equation is:

$$\frac{d(Te^{\phi})}{dr} = -\frac{-3k\rho L_{\gamma} e^{\phi}}{16\sigma T^3 4\pi r^2 (1-2GM/rc^2)} \tag{2.34}$$

here κ is total opacity, which is determined by the radiative opacity and the heat conductivity through the relation:

$$\frac{1}{k} = \frac{1}{k_R} + \frac{1}{k_c} \quad , \tag{2.35}$$

here κ_R stands for the radiative transfer opacity and κ_c is the opacity due to heat conductivity.

The conductive opacity

$$k_c = \frac{4acT^3}{3\rho\lambda} \quad , \tag{2.36}$$

with $a = \frac{4\sigma}{c}$ where σ is Stefan-Boltzmann constant.

The radiative opacity can be divided into three parts:

$$\kappa_r = \kappa_{bf} + \kappa_{ff} + \kappa_{es} , \tag{2.37}$$

where κ_{bf} is the opacity due to the bound free transition, κ_{ff} is the opacity due to the free-free transition and k_{es} is the opacity due to the electron scattering.

The conductive opacity k_c is completely dominated by the contribution from electrons and neutrons. There are four processes which contribute to κ_c: the electron-electron scattering κ_{ee}, the electron-impurity scattering k_{ei}, the electron-phonon scattering κ_{ep} and the electron-neutron scattering k_{en}. In the low density region ($\rho<1.04\times10^4 g/cm^3$), heat conductivity is of a nonrelativistic, degenerate gas (Clayton D., 1983).

Total opacity then is calculated as:

$$\frac{1}{k} = \frac{1}{k_R} + \frac{1}{k_c} = \frac{1}{k_{bf} + k_{ff} + k_e} + \frac{1}{k_c} \tag{2.38}$$

2.3.6 Effect of Heating

For ordinary isolated neutron stars and pulsars where surface magnetic fields do not exceed $\sim 10^{13}$ Gauss, the only heating mechanism which can seriously affect cooling is the frictional heating which takes place in the inner crust. Neutrons there are expected to be in a superfluid state. Then, as the star is spinning down, while the rigid crustal heavy ions spin down with the star superfluid neutrons will not. Therefore, there arise frictions between the heavy ion crustal material and superfluid neutrons which cause heating. The efficiency of this frictional heating depends on how strongly the superfluid vortex is pinned to the crust, and hence the strength of this pinning determines heating (Umeda H. et al., 1993; Tsuruta S., 1998). See also Appendix B for vortex pinning velocities calculation. The heating term H is expressed as:

$$H = 1.27\times10^{4}(t+\tau_0\,(yr))^{-3/2}\ K\ (ergs\ m^{-3/2}\ s^{2})\ ergs\ s^{-1}, \qquad (2.39)$$

where t is the age of the star, τ_0 is spin-down time at $t = 0$, and K is strength of vortex creep pinning.

Typical examples are shown in Figure 2.7, where the surface temperature T_s^{∞} (to be observed at infinity) is plotted vs. age t, for stiff PS Model, introduced in the section 2.2. The solid curve represents cooling without heating. The upper three curves refer to models with frictional heating included, with varied degrees of heating. The uppermost curve (long dashed) refers to the maximum heating expected from the frictional heating theory. The downward arrows represent upper limits for the temperatures of neutron stars and vertical error bars are referred to detections of surface temperatures observed from some neutron stars (e.g. Vela pulsar 0833-45, PSR (0656+14 etc.).

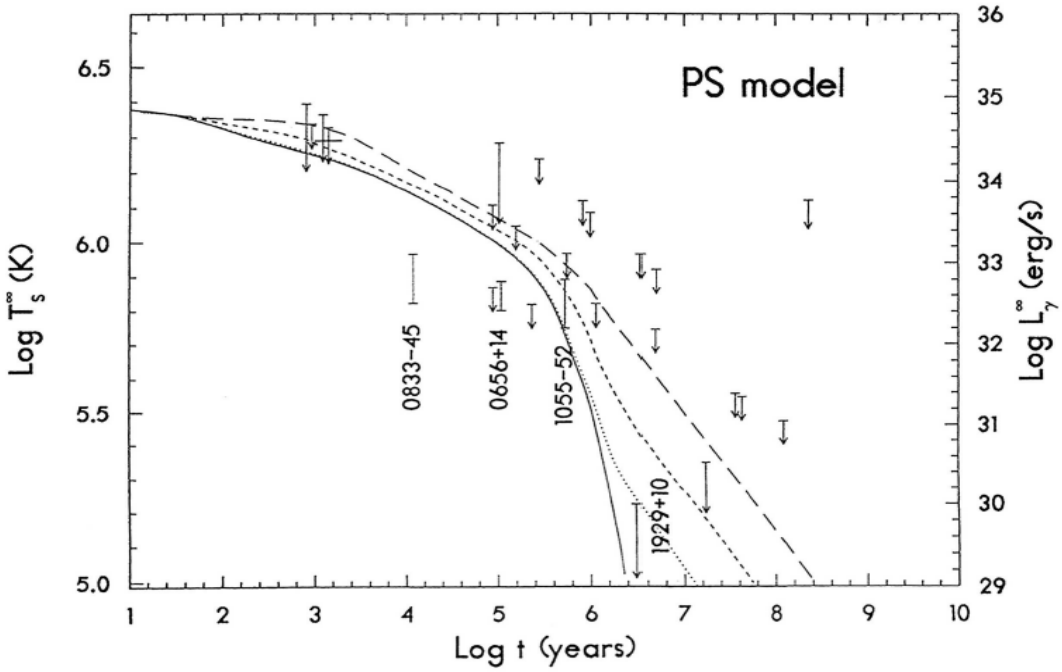

Figure 2.7. The effects of frictional heating on neutron star cooling (Tsuruta S., 1998).

In this section, we introduced the main physical inputs necessary for thermal calculations of neutron stars. So far we have neglected the effects of magnetic fields on the opacities. The magnetic field causes anisotropy of opacities, causing the temperature variations over the surface, and changes the core-surface temperature relation. This effect becomes important for magnetars with $H > 10^{13}$ Gauss, but not for pulsars considered here.

CHAPTER 3

QUARK MODEL

3.1. Quark Matter Theory

The theoretical understanding of the neutron star structure requires the knowledge of the equation of state of highly compressed cold hadronic matter, up to densities of $\rho_c = 1.7$ fm^{-3} (Shapiro, Teukolsky, 1983), where density is given in the units of *neutrons per fm^{-3}* and in CGS units it is equal to ~ 1×10^{15} g/cm^3.

Unit calculation:

$$1\,fm^{-3} = \frac{1}{\left(10^{-13}\,cm\right)^3} \tag{3.1}$$

The density of free neutrons in the hadronic matter is expressed as 1.7 neutrons per $(10^{-13}\text{cm})^3$ or, using mass of a neutron $m_n=1.675\times10^{-24}$g,

$$\rho_c = 1.7\times\left(1.675\times10^{-24}\,g\right)\times\frac{1}{\left(10^{-13}\,cm\right)^3} \approx 1\times10^{15}\,g/cm^3 \tag{3.2}$$

In such an extreme environment the appearance of "exotic" components of matter such as hyperons, meson condensates and quark matter is expected. The models with hyperon and meson condensates in the core of neutron star were reviewed thoroughly by Tsuruta (1998, 2010), while the theoretical description of quark matter was limited by large uncertainties in EoS, superfluid properties, etc. Calculations of neutron star structure based on a nucleonic equation of state, show that for heavy neutron stars, close to the maximum mass (about two solar masses) the central density ρ_c reaches values

larger than 10^{15} g/cm^3. In this density range nucleons in the core, whose dimensions are about 0.5×10^{-13} cm, and start to touch each other. It can be expected that the nucleons start to lose their identity and quark degrees of freedom are excited at a microscopic level.

In this work we will try to adopt some phenomenological models of EoS for the quark matter and constrain it by the experimental information available on high-density hadronic matter.

3.1.1 Quarks

A quark, an elementary particle and a fundamental constituent of matter, was proposed in 1964 by Gell-Mann M. and Zweig G. independently (Gell-Mann M., 1964; Zweig G., 1964). Quarks combine to form composite particles called hadrons, the most stable of which are protons and neutrons, the components of atomic nuclei (Griffiths D., Introduction to elementary particles, 1987).

The quark model asserts that:

- Every baryon is composed of three quarks (and every antibaryon is composed of three antiquarks).
- Every meson is composed of a quark and an antiquark.

The quarks come in six types or "flavors" named up (u), down (d), strange (s), charm (c), bottom (b), and top (t) (Table 2.2).

Table 3.1. Quark flavor properties.

Name	Symbol	Mass, MeV/c^2	J	B	Q	I_3	Antiparticle	Antiparticle symbol
First generation								
Up	u	1.7 to 3.3	$\frac{1}{2}$	$+\frac{1}{3}$	$+\frac{2}{3}$	$+\frac{1}{2}$	Antiup	u
Down	d	4.1 to 5.8	$\frac{1}{2}$	$+\frac{1}{3}$	$-\frac{1}{3}$	$-\frac{1}{2}$	Antidown	d
Second generation								
Charm	c	1,270	$\frac{1}{2}$	$+\frac{1}{3}$	$+\frac{2}{3}$	0	Anticharm	c
Strange	s	101	$\frac{1}{2}$	$+\frac{1}{3}$	$-\frac{1}{3}$	0	Antistrange	s
Third generation								
Top	t	172,000	$\frac{1}{2}$	$+\frac{1}{3}$	$+\frac{2}{3}$	0	Antitop	t
Bottom	b	4,190	$\frac{1}{2}$	$+\frac{1}{3}$	$-\frac{1}{3}$	0	Antibottom	b

Here: J = total angular momentum, B = baryon number, Q = electric charge, I_3 = isospin.

Up and down quarks have the lowest masses of all quarks. The heavier quarks change into up and down quarks through a process of particle decay: the transformation from a higher mass state to a lower mass state. Because of this, up and down quarks are generally stable which leads to the stability of hadrons that are made up of these flavors, such as protons and neutrons.

Quarks are spin-½ particles, implying that they are fermions and are subject to the Pauli Exclusion Principle, which states that no two identical fermions can simultaneously occupy the same quantum state.

The Pauli Exclusion Principle brings the notion of quark color into consideration. The baryons are bound states of three quarks:

$$p = uud \tag{3.3a}$$

$$n = udd \tag{3.3b}$$

$$\Delta^{++} = uuu \tag{3.3c}$$

According to the Δ^{++} baryon, the quark scheme forces us to combine three identical fermions u in a completely symmetric ground state *uuu*. But such a state is forbidden by Fermi statistics. The problem is solved by introducing a new quantum number for quarks: color. The quarks are supposed to come in three primary colors: red (R), green (G) and blue (B); and the color wavefunction for a baryon is:

$$(qqq)_{singlet} = (RGB - RBG + BRG - BGR + GBR - GRB) \tag{3.4}$$

where the antisymmetric character of the total wave function is achieved; it is overall symmetric in space, spin, flavor structure and antisymmetric in color (Halzen F., Martin A., "Quarks and leptons", 1984).

The color charge is a property of quarks and gluons that is related to the particles' strong interactions in the theory of quantum chromodynamics. The system of attraction and repulsion between quarks charged with different combinations of the three colors is called the strong interaction, which is mediated by a force carrying particles known as

gluons. A quark charged with one color value can form a bound system with an antiquark carrying the corresponding anticolor; three (anti)quarks, one of each (anti)color, will similarly be bound together. The result of two attracting quarks will be color neutrality.

Under sufficiently extreme conditions, quarks may become deconfined and exist as free particles. This is similar to the structure of matter, where the basic constituents are nuclei and electrons, is disrupted. In quark matter it is more appropriate to treat the quarks themselves as the basic degrees of freedom.

It is believed that at high densities the quark matter is a more stable configuration than the ordinary nuclear matter (Rodrigues H. et al., 2010), and hence neutron stars are expected to consist of quark matter partially or completely and these stars are called hybrid stars. The value of the maximum mass of a neutron star is sensitive to the presence of quark matter. If the quark matter EoS is sufficiently soft, the quark component is expected to appear in neutron stars and affect the mass value. The purely nucleonic equations of state are able to accommodate the maximum mass values. In the presence of quark matter it would be possible to stiffen the EoS and reach large neutron star masses (Chen H. et. al., 2011). Therefore, heavy neutron stars could be hybrid stars with a quark core.

3.1.2 Different Quark Models Used for Neutron Stars.

Some equations of state used in describing quark matter are too soft to support stars with large masses and are inconsistent with observational data (Cottam L. et.al, 2002). The density-dependent quark mass model provides a stiff equation of state and

hence large quark star masses can be obtained if reasonable values for the EoS parameters are used. Calculations of compact star models using quark matter EoS, such as the MIT bag model, the Color Dielectric Model (CDM) or the Nambu-Jona-Lasinio (NJL) model are capable of describing a maximum limit for mass of around $2M_{\odot}$, which is compatible with observations (Rodrigues H. et al, 2010).

The MIT bag Model provides a useful phenomenological description of quarks being confined inside hadrons (Maieron C. et al., 2004). Quarks are treated as massless particles inside a bag of finite dimension. They are infinitively massive outside the bag. Confinement results from the balance of the pressure on the bag walls from the outside and the pressure resulting from the kinetic energy of the quarks inside the bag. The bag pressure constant, B, is related to the equilibrium radius of the bag:

$$B^{1/4} = \left(\frac{6.12}{4\pi}\right)^{1/4} \frac{1}{R} \tag{3.5}$$

For a baryon radius of R=0.8 fm, $B^{1/4}$=206 MeV. Inside the bag perturbative quantum chromodynamics (QCD) applies. The total color charge of the matter inside the bag must be colorless, thus valid hadronic bags can only contain *qqq* and qq states.

The Color Dielectric Model (CDM) has been originally used to study both the static and the dynamical properties of the nucleon. In the CDM model the nucleon is described as a soliton in which quarks are dynamically confined via the interaction with scalar-isoscalar singlet field. The CDM has been also applied in the quark sector to calculate the EoS of quark matter (Maieron C. et al., 2004). Applications of the CDM EoS for quark matter to the study of compact stars have been considered by Ghosh S. et

al. (1995) and by Drago A. and collaborators (1995), who studied the structure of hybrid stars and the problem of supernova explosions.

A model based on the *Dyson-Schwinger equations* of QCD is adopted for the deconfined quark phase, and provides a continuum approach to QCD that can simultaneously address both confinement and dynamical chiral symmetry breaking. It has been applied with success to hadron physics in vacuum but recently efforts have been made to calculate the EOS for cold quark matter and compact stars (Chen H. et al., 2011).

The *Nambu–Jona-Lasinio Model* is a theory of nucleons and mesons constructed from interacting Dirac fermions with chiral symmetry which parallels the construction of Cooper pairs from electrons in the BCS theory of superconductivity. According to the theory, electrons near the Fermi surface can form Cooper pairs due to the electron phonon interaction. These pairs undergo condensation and completely alter the nature of the ground state of the superconductor. In fact, the model was much inspired by recent progress in the different field of solid state theory (Klevansky S., 1992).

In this work we will not consider these and other quark matter models more precisely, but will compare the estimated mass, radius and transition density phases for different models.

To consider the hadron-quark phase transition in neutron stars, we refer to Figure 3.1, which determines the range of central density where both baryonic and quark matter coexist. The solid curve refers to the EoS of nuclear matter, the dashed line represents the EoS of beta-stable and charge neutral (u, d, s) quark matter obtained within the CDM, and the dotted and dot-dashed lines are the results due to the MIT bag model with

constant and density dependent B, respectively. Markers indicate the crossing points between the hadron and the quark phases. We notice that the phase transition from hadronic to quark matter occurs at very low baryonic density when the CDM is used to describe the quark phase, whereas higher values of the transition density are predicted with the MIT bag model.

In Figure 3.2 and Figure 3.3 the possible effects of the hadron-quark phase transition on mass and radius for different models is shown. The gravitational mass M_G (in units of the solar mass*)* is plotted as a function of the radius R and central baryon density ρ_c. Among the given EoS the DS (Dyson-Schwinger) model is closest to our Best Buy Model in terms of mass-radius-density relationship. For Best buy model the transition density is $\rho_{tr} = 4\rho_0 = 1.12 \times 10^{15}$ g/cm^3 and corresponding mass is ~ $1.8M_\odot$.

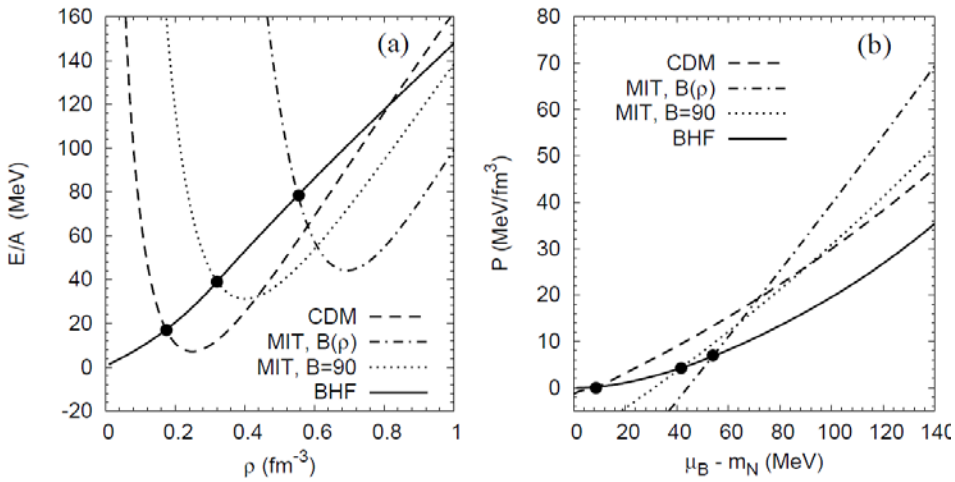

Figure 3.1. Energy per particle vs. baryon density for beta-stable hadronic matter (solid line) and for u, d, s quark matter obtained within the MIT model (dotted and dot-dashed lines) and the CDM model (dashed line) (Maieron C. et al., 2004).

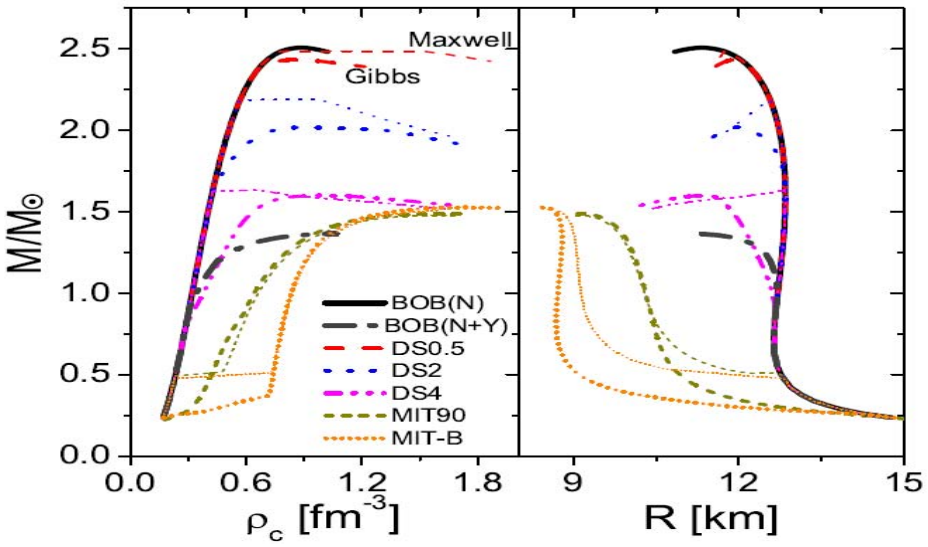

Figure 3.2. Gravitational neutron star mass vs. radius (right panel) and central baryon density (left panel) for different EoS (Chen H. et al., 2011).

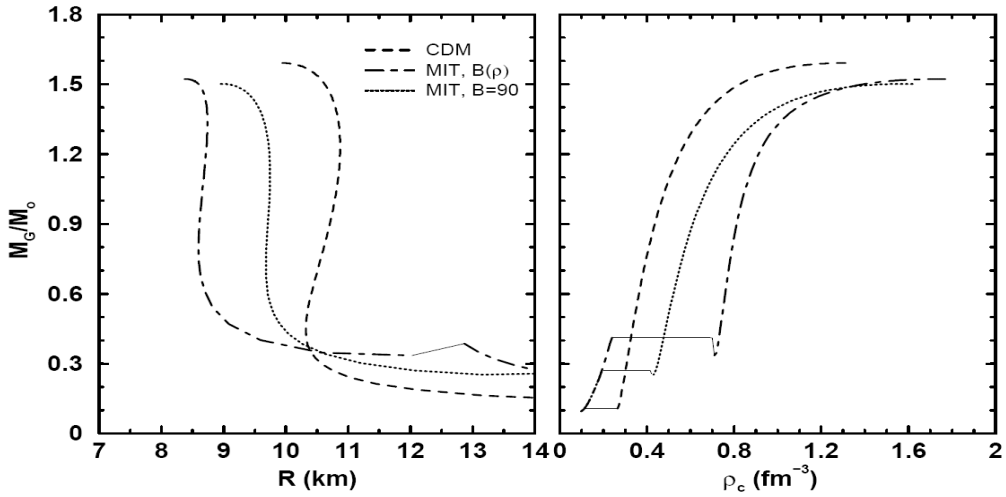

Figure 3.3. Gravitational neutron star mass vs. radius (left panel) and central baryon density (right panel) for CDM, MIT bag model EoS (Maieron C. et al., 2004).

3.2 Neutrino Emission Processes in Quark Matter

The physical reason for the high neutrino luminosity in the core of a hybrid star is that while in ordinary neutron star interior the direct beta decay and capture processes are prohibited due to the momentum conservation law, this direct decay process in the quark matter can occur.

We consider three-component quark matter (u, d, s) in β-equilibrium the conditions for which is (Iwamoto N., 1980):

$$\mu_d = \mu_s = \mu_u + \mu_e, \tag{3.6}$$

where $\mu_{d,}$ μ_s, μ_u and μ_e are chemical potentials of quarks and an electron. If we assume the quarks to be noninteractive and massless, each quark momentum component p_F (i) would have the same Fermi momentum:

$$p_F(i) = 235(\rho/\rho_0)^{1/3}\ MeV/c, \tag{3.7}$$

where ρ_0 is the nuclear density.

The main β-decay reactions are considered to happen due to the β-decay and capture of u and d flavor quarks.

$$u + e^- \rightarrow d + \nu_e \tag{3.8}$$

$$d \rightarrow u + e^- + \overline{\nu_e} \tag{3.9}$$

At low temperatures the momenta of emitted neutrinos are small and quarks and electrons all lie near their respective Fermi surfaces, and this requires that we can

construct a triangle from momenta of magnitudes $p_F(u)$, $p_F(d)$ and $p_F(e)$ taking into account a weak quark-quark interaction. Constructing the momentum triangle we can imply that the equations of quark beta decay (3.8) are allowed to proceed.

The transition rate for beta-decay of d quark is:

$$W_{fi} = \frac{V(2\pi)^4 \sigma^4 (p_1 - p_2 - p_3 - p_4)|M|^2}{\prod_{i=1}^{4} 2E_i V}, \qquad (3.10)$$

where the four-vectors $p_i = (E_i,)$ denote those of d, , u and e, relatively. V is the normalization volume and $|M|^2$ is the squared invariant amplitude averaged over the initial d-quark spin (σ_1) and summed over the final spins of u quark (σ_3) and electron (σ_4):

$$|M|^2 = \frac{1}{2}\sum_{\sigma_1,\sigma_2,\sigma_3} |M_{fi}|^2 = 64G^2 \cos^2\theta (p_1 \cdot p_2)(p_3 \cdot p_4), \qquad (3.11)$$

where $G = 1.435 \times 10^{-49}$ erg cm^3 is the weak-coupling constant.

When quark masses and interactions are neglected, the $|M|^2$ vanishes.

The emissivity of the processes (3.8) and (3.9) is given by the formula:

$$\varepsilon_q = \frac{914}{315} \frac{G^2 \cos^2\theta}{\hbar^{10} c^6} \alpha_c p_F(d) p_F(e) (k_B T)^6, \qquad (3.12)$$

where temperature dependence T^6 is explained by the contribution of one power of T from each quark and electron (from the phase-space integral), and the phase-space integral for neutrinos gives also $\propto T^3$. Altogether, we thus have $\varepsilon_q \propto T^6$ (Iwamoto N., 1980).

Thus, the estimated magnitude of neutrino emissivity during the direct quark beta decay is:

$$\varepsilon_q \cong 8.8\times10^{26}\alpha_c\left(\rho/\rho_0\right)Y^{1/3}T_9^6, \tag{3.13}$$

where $Y = n_e/n_b$ is the number of electrons per baryon and T_9 is the temperature in units of 10^9 K (Iwamoto N., 1980).

This quark neutrino emissivity is much larger than that of ordinary neutron star matter. The neutrino emissivity from nucleon-modified URCA processes (2.23) and (2.24) is (Iwamoto N., 1980):

$$\varepsilon_{URCA} \cong 1.8\times10^{21}\alpha_c\left(m_n^*/m_n\right)^3\left(m_p^*/m_p\right)\left(\rho/\rho_0\right)^{2/3}T_9^8, \tag{3.14}$$

Here m^*_n and m^*_p are the neutron and proton effective masses.

In the nucleon modified URCA process the number of participating degenerate fermions is larger by a factor of 2 than for process (3.8), which leads to tighter phase-space restrictions and lower emissivity of the modified URCA process.

CHAPTER 4

OUR PHYSICAL MODEL

We adopted a neutron star model which is based on recent studies of nuclear theories and observational data, using a general relativistic "exact evolutionary code" which was originally constructed by Nomoto & Tsuruta in 1987.

The equation of state adopted is TNI 6, a model of medium stiffness, where the nucleonic matter transforms to quark matter at transition density $\rho_{tr} = 4\rho_0$ (here $\rho_0 = 2.8\times10^{14}$ g/cm^3). Nonstandard cooling involving a hyperon-mixed core and a core with pion condensates are already calculated by S. Tsuruta et al. (2009) and (2010). Another possibility for non-standard cooling involves the presence of nonhadronic quark matter in the interior of neutron stars. Since that option has not been explored in detail, here we explore that option as a nonstandard cooling scenario.

The general properties of different EoS are shown in Table 4.1 where R, R_e, M, M_p, ρ_c, ε_c and P_c are stellar radius, effective radius (to be observed at infinity), proper mass (baryonic mass), gravitational mass (observed mass), central matter density (sum of number density times rest mass of constituent particles), central energy density (mass density including gravitational and nuclear forces), and pressure, respectively.

In this model neutron stars with masses lower than 1.45 $M_\odot$ are considered to undergo the standard cooling scenario where modified URCA processes dominate, but all other possible standard cooling mechanisms, such as neutrino bremsstrahlung and plasmon neutrinos, are also included (Tsuruta S. et.al, 2009).

Table 4.1 Properties of TNI 6 Model (Tsuruta S. et.al, 2009).

EoS	R	R_e	M_p	M_G	ρ_c	ε_c	P_c
TNI 6	11.162	13.675	1.4	1.26	15.018	15.06	35.155
	10.911	13.904	1.6	1.42	15.093	15.14	35.338
	10.867	13.937	1.63	1.44	15.106	15.159	35.367
	10.800	13.976	1.67	1.47	15.123	15.180	34.409
	10.676	14.019	1.73	1.52	15.152	15.214	35.476
	10.633	14.041	1.75	1.53	15.162	15.226	35.500
	10.610	14.101	1.76	1.54	15.167	15.230	35.512
	10.350	14.101	1.85	1.6	15.290	15.451	35.782

For higher mass stars we adopted quark cooling, as an example of non-standard fast neutrino cooling which can be suppressed significantly by superfluidity. The main important cooling mechanism is quark direct URCA processes (3.12).

As to superfluidity of constituent particles, neutrons in the inner crust are expected to be in the $^1S_0$ superfluid state. For quarks we adopt a superfluid model with a density-dependent energy gap (modified HGRR model) which corresponds to a more realistic pattern with corresponding critical superfluid temperature T_{cr} peaking at ~ 10^9 K.

For our heating calculations we adopt the vortex creep heating model (Tsuruta S., 1998). The heating term H is added to the standard energy balance equation (2.6) which balances the rate of loss of internal energy to neutrino and photon emissions. It is expressed as in Chapter 2, equation (2.39):

$$H = 1.27\times10^{4}(t+\tau_0\,(yr))^{-3/2}\ K\ (ergs\ m^{-3/2}\ s^{2})\ ergs\ s^{-1}, \qquad (4.1)$$

where t is the age of the star, τ_0 is spin-down time at $t = 0$, and K refers to the measure of strength of vortex creep pinning which can be expressed as:

$$K = 10^{37.5} I^{1/2}{}_{45}\, I_{s45}\, \omega 0/B_{12}\, \sin\beta R^{3}{}_{10}\ ergsm^{-3/2}\ s^{2}, \qquad (4.2)$$

where I_{45} and I_{s45} are the moment of inertia of the whole star and that of the neutron superfluid in the inner crust, respectively, in the units of 10^{45} g cm^2, ω_0 is the average value of the angular velocity difference between the inner crust neutron superfluid and the crust itself, B_{12} is the magnetic field in the units of 10^{12} Gauss, β is the angle between the rotation and magnetic axes, and R_{10} is the stellar radius in the units of 10 km. We adopt in our calculations B=10^{12} Gauss, reasonable for ordinary pulsars (Tsuruta S., 1998).

The effect of magnetic fields on cooling is not included though as we were restricted to isolated pulsars (not magnetars), where the magnetic fields are less than ~ 10^{13} Gauss.

4.1 Our Theoretical Model and Results.

Figure 4.1 shows thermal evolution of neutron stars for TNI 6 models with EOS of medium stiffness and mass range between 1.4 $M_\odot$ and 1.9 $M_\odot$. On this figure photon luminosity to be observed at infinity is shown as a function of age t. The upper solid

curve refers to stars with gravitational mass of M=1.4 $M_\odot$ with moderate heating with the heating parameter K = 10^{36} ergs $m^{-3/2}$ s^2. For the star of this mass the central density $\rho_c < \rho_{tr}$, and the star would go through standard cooling.

The rest of the curves correspond to nonstandard cooling of 1.5 $M_\odot$, 1.6 $M_\odot$, 1.65 $M_\odot$, 1.9 $M_\odot$ stars with a quark core, respectively, all without heating, but with superfluidity included. In our model, the stars with mass larger than 1.4 $M_\odot$ are considered to have a quark core and are subject to nonstandard quark direct URCA process.

Note that after the superfluidity appearance the critical temperature T_{cr} first increases, reaches a peak and then decreases with density increase (see Figure 2.5 for HGRR density-dependent energy gap model). Therefore, according to Equation (2.33) the most massive star of 1.9 $M_\odot$ cools very fast because the central density is so high that quark superfluidity in the core disappears. For the intermediate stars with 1.5 $M_\odot$, 1.6 $M_\odot$, 1.65 $M_\odot$ the superfluid suppression is still effective.

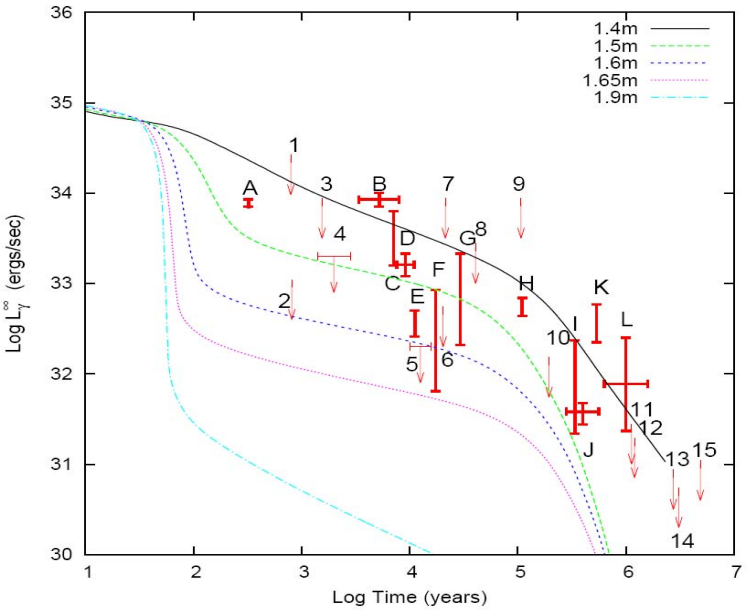

Figure 4.1. Thermal evolution of neutron stars with TNI6 EOS, of medium stiffness. The upper solid curve refers to a star with gravitational mass $M = 1.4\ M_\odot$, with medium vortex creep heating with heating parameter of $K = 10^{36}$ ergs $m^{-3/2}$ s^2. The rest of the curves (the lower four curves) represent nonstandard quark cooling of stars with gravitational mass of 1.5 $M_\odot$, 1.6 $M_\odot$, 1.65 $M_\odot$, and 1.9 $M_\odot$, respectively, all without heating, in the order of decreasing luminosity. The observation data for various sources are shown as bars and crosses for surface temperature and slow down rate detection, and downward arrows for the temperature upper limits (see tables 4.2 and 4.3).

4.2 Observational Data

The observational data for various sources are shown as bars and crosses for detection and downward arrows for upper limits (see tables 4.2 and 4.3).

Table 4.2. Neutron star luminosity detection for various sources.

Source	$\log_{10}$ t (age)	$\log_{10}$ (ergs s^{-1})	Reference
A RX J0822 – 4247 (Puppis A)	3.53 – 3.90	33.85 – 34.00	Zavlin et al., 1999
B RX J0002 + 6246	3.88 – 4.04	33.08 - 33.33	Page et al., 2004
C PSR 0833 – 45 (Vela)	4.04	32.41 – 32.70	Pavlov et al., 2001
D PSR 1706 – 44	4.24	31.81 – 32.93	McGowan et al., 2004
E PSR 0538 + 2817	4.47	32.32 – 33.33	Zavlin&Pavlov, 2004
F PSR 0656 + 14	5.04	32.64-32.84	Pavlov et al., 2002
G PSR 0633 + 1748 (Geminga)	5.53	31.34 – 32.37	Kargaltsev et al., 2005
H RX J1856.5 - 3754	5.45 – 5.75	31.44 – 31.68	Pons et al., 2002
I PSR 1055 - 52	5.75	32.35 – 32.77	Steiner&Reddy, 2008
J RX J0720.4 - 3125	5.8 – 6.2	31.37 – 32.40	Motch et al., 2003

Table 4.3. Neutron star luminosity upper limits for various sources.

Source	$\log_{10}$ t (age)	$\log_{10}$ (ergs s^{-1})	Reference
1 CXO J232327.8 + 584842 (Cas A)	2.51	34.5	Pavlov et al., 2000
2 PSR B 0531+21 (Crab)	2.9	34.45	Weisskopf et al., 2004
3 J0205+6449 (3C58)	2.95	33.0	Slane, 2004
4 PSR B1509-58 (MSH – 15-52)	3.19	33.9	Becker & Pavlov et al., 2002
5 PSR J1124-5916 (G292+1.8)	3.15 – 3.45	33.3	Hughes et al., 2003
6 RX J0007 + 7303 (CTA I)	4-4.2	32.3	Halpern et al., 2004
7 PSR B1046 -58 (Vela Twin)	4.31	32.7	Becker & Pavlov et al., 2002
8 PSR B1823 – 13 (Vela like)	4.33	33.9	Becker & Pavlov et al., 2002
9 PSR B2334+61	4.61	33.4	Becker & Pavlov et al., 2002
10 PSR B1951 +32 (CTB 80)	5.03	33.9	Becker & Pavlov et al., 2002
11 PSR J0154+61	5.29	32.14	Gonsaltz et al., 2004
12 PSR B2224+65	6.053	31.4	Becker et al., 2009
13 PSR J2043+2740	6.08	31.25	Becker et al., 2009
14 PSR B0628-28	6.44	30.9	Becker et al., 2009

Table 4.3 Continued. Neutron star luminosity upper limits for various sources.

15 PSR B1929+10	6.49	30.7	Becker et al., 2009
16 PSR B0823+26	6.69	31.0	Becker & Pavlov et al., 2002

A breakthrough in the neutron star cooling-related area came in the 1990s when ROSAT reported, for the first time, the detection of neutron star surface temperatures, not just the upper limits, for at least three pulsars, PSR0656+14, PSR 1055–52, and PSR 0633+1748 (Geminga), and possibly PSR0833-45 (Vela pulsar) also. Therefore, more comprehensive investigations of cooling and related problems were carried out. For instance, Umeda et al. (1993), (1994) included, for the first time, the effect of the frictional heating. Umeda et al. (1994) and Umeda, Tsuruta and Nomoto (1995), investigated the effects of superfluidity, stellar mass, EOS, heating, and different versions of nonstandard direct URCA cooling, with nucleons, pion, kaon, and kaon + pion condensates, and quarks, in more thorough ways, adopting fully general relativistic exact evolutionary code. In these calculations the most up-dated input microphysics which were available at the time, the improved version of the earlier microphysical input in Nomoto and Tsuruta (1987) were adopted. In order to compare different nonstandard models, a simple assumption was adopted that the transition to all of these different 'exotic' nonstandard processes takes place at the same density $\rho_{tr}= 4\rho_0$, (where $\rho_0= 2.8\times10^{14}$ g/cm^3 is the nuclear density).

We introduce the NS cooling data updated as of 2008 March. There are 11 isolated NSs with possible detection. These are: (A) RX J0822−4247 (in Puppis A), (B)

1E 1207.45−5209, (C) RX J0002+6246, (D) PSR 0833−45 (Vela pulsar), (E) PSR 1706−44, (F) PSR 0538+2817, (G) PSR 0656+14, (H) PSR 0630+1748 (Geminga), (I) RX J1856.5−3754, (J) PSR 1055−52, and (K)RX J0720.4−3125.11.

Their properties and references are listed in Table 4.2. Here t is the age and is the total surface photon luminosity to be observed at infinity.

There about two dozen upper limits are known. However, some are not interesting as they are too high above the cooling curves to constrain cooling theories and/or too old. We choose 16 which are either better known sources (e.g., pulsars in Crab and Cas A) or more interesting for our purpose of constraining theories. They are listed in Table 4.3. The notations used are the same as in Table 4.2. Among these, more interesting sources are: (1) CXO J232327.8 (Cas A), (2)PSR 0531+21 (Crab pulsar), (3) PSR J0205+6449 (in 3C 58), (4) PSR 1124−5916 (in G292.0+1.8), (5) PSR 1509−58 (in MSH-15−52), (6) RX J0007.0+7302 (in CTA 1), (7) PSR 1046−58 (Vela twin), (8) PSR 1823−13 (Vela-like), (12) PSR 2224+61, (13) PSR 2043+2740, (14) PSR 0628−28, (15) PSR 1929+10, and (16) PSR B0823+26. PSR J0205+6449 in 3C 58 and RX J0007.0+7302 in CTA 1 are especially important because they are relatively cold and they probably will require nonstandard cooling.

Among these neutron stars the precise age is known only for the Crab, as its historical age. Other ages have to be estimated.

The horizontal error bars refer to the pulsar spin-down age (minimum) and kinetic age (maximum) when both are known.

It may be noted that by comparing cooling/heating theoretical curves with observed data, it is more preferable to choose the surface photon luminosity (to be observed at infinity) L_γ versus age t relation, rather than the temperature versus age. Sometimes we can have different interpretation and conclusion when we adopt these two different methods (luminosity or temperature). The major reason is: observers estimate luminosity L_γ from the observed flux, distance, and normalization, while temperature is determined from flux, stellar radius, and normalization. Theorists, however, first obtain luminosity and convert it to temperature, adopting a blackbody relation that depends on the square of radius R, which also can be effected by some hydrogen contamination or/and magnetic fields. Moreover, both mass and EoS from theories depend on R (e.g., smaller R for soft EoS). We normally show theoretical curves with various EoS and mass (with different R) on the same graph, which are compared with observed data points. Since we use a fixed R to derive temperature while different theoretical curves refer to different R, the method of adopting temperature is often not accurate. However, both theoretical and observed luminosity are independent of R. Therefore, when distance is known, comparing luminosities is a more direct and correct method for testing theory by comparing it with observation.

4.3 Discussion

Summarizing our result with our theoretical models and observational data, we see that:

- With increasing mass (and hence central density) cooling curves decrease smoothly from the standard cooling of less massive stars to the nonstandard quark cooling of more massive stars, due to the density dependence of the superfluid energy gaps (the gap almost disappears when the density is very high). The lower mass and hence less dense stars undergo standard cooling since their central density is lower than the transition density ρ_{tr}, and higher mass stars' densities exceed the transition density ρ_{tr} and they are going through non-standard quark cooling.
- As an effect of EoS we can say that the transition to quark matter happens for lower mass stars for softer EoS. For example, for a soft EoS, the critical mass is M=1.26 $M_{\odot}$ and for medium EoS it is M=1.4M $M_{\odot}$.
- We adopted a density-dependent superfluid energy gap for quark superfluidity which is a relatively new approach in thermal calculations for quark-mixed core stars. The comparison with related current research made by other theorists in this field is to be discussed in the next section.
- We note that all of the nonstandard mechanisms are too fast to be consistent with observations of cool stars, such as Vela pulsar. Therefore, we require nonstandard neutrino emissivity to be significantly suppressed by quark superfluidity in the core.
- The main nonstandard cooling mechanism is direct URCA cooling involving such exotic states as pion condensates, hyperon contamination or quark matter. Our results show that the direct URCA cooling due to the quark core is

consistent with the observation provided that the quark models presented are valid.

4.4 Comparison with Other Quark Cooling Neutron Star Work

Here we compare the results we obtained for quark cooling with the results by other research groups, such as Blaschke D. et al. (2004).

Blaschke D. et al (2004) have investigated the thermal evolution of quark core neutron star. Their results have some similarities with ours in general microphysical input and general cooling mechanisms, but differ in cooling curves obtained.

The similarities with our research are as follows. The authors used the HHJ EOS, which is based on nucleon-nucleon interaction and with the inclusion of three-body force for nucleon-quark hybrid stars. As a cooling mechanism for a quark core they included the quark Direct URCA processes on unpaired quarks, the quark modified URCA, and the quark bremsstrahlung as main processes.

The significant difference of their work from ours is in using a different model for superfluid energy gap of weakly paired quarks, which was considered to be density-independent and equal to ~ 50 keV.

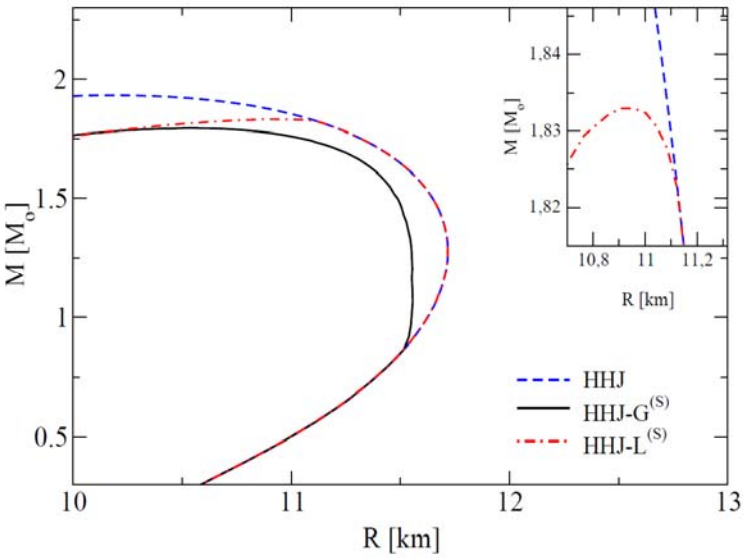

Figure 4.2. Mass - radius relations for compact star configurations with different EoS: purely hadronic star with HHJ EoS (dashed line), stable hybrid stars with HHJ - SM(S) G EoS (solid line) and with HHJ - SM(S) L EoS (dash-dotted line) (Blaschke D. et al, 2004).

The cooling curves are presented in Figure 4.3. They showed that the choice of a constant weak pairing gap could be a reason for the narrow mass intervals in the intermediate cooling data (so-called fine tuning in mass) and that to be more realistic one should further include density dependence of the gaps. In our work we included density-dependent energy gap and had the cooling curves spaced more evenly and realistic.

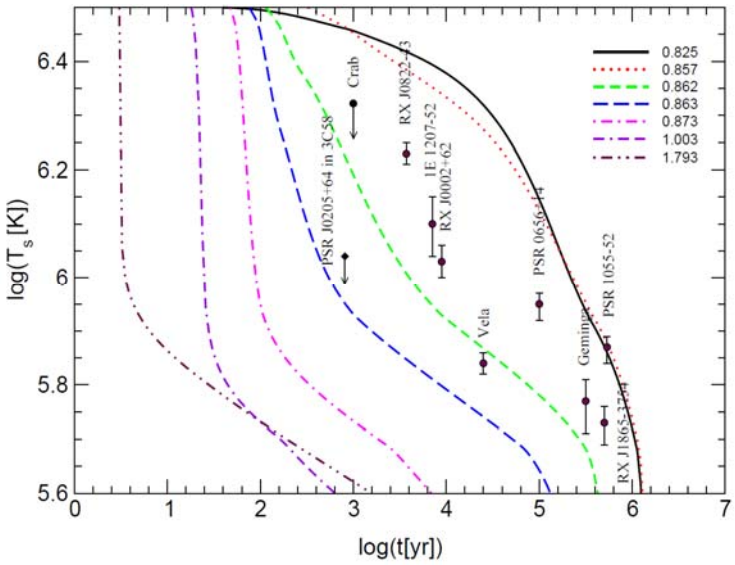

Figure 4.3. Cooling curves for hybrid star configurations with a quark core in the superconducting phase. The labels correspond to the gravitational masses of the configurations in units of the solar mass (Blaschke D. et al., 2004).

CHAPTER 5

CONCLUDING REMARKS

5.1 Future Prospects

Some of our research work presented here might be still in progress due to various uncertainties, both in theory and observation. However, this situation will change if we succeed in achieving some improvements, which appear to be within our reach in the foreseeable future. For instance:

• Among all existing theoretical models some are consistent with observations better than others. This study helps to constrain theoretical models.

• Continuation of such new theoretical studies of nuclear and elementary particle physics will help us distinguish between different models. That will also open opportunities for more realistic studies of quark cooling than currently available.

• Next generation X-ray space missions, such as ASTR-H, will offer more observations with less uncertainties and better estimate of upper limits. The detections and upper limits to be obtained by these missions will be important especially for the fainter sources currently out of our reach.

• More precise determination of distance can reduce uncertainties in measurements. We have already noted that using surface photon luminosity for cooling curves is more accurate than using temperatures when testing cooling/heating theories with observation if distance is accurately known. In fact, luminosity error bars for some pulsars, e.g. PSR0656+14, were reduced significantly already due to recent success of

direct radio parallax measurements of the distance by VLBI (Very Long Baseline Interferometry). Larger radio array systems planned for the future, e.g. SKA (Square Kilometer Arrays), will improve direct distance measurements for more objects.

5.2 Conclusion

Thereby, in Chapter 2 we have reviewed the main physical parameters, such as the equation of state, superfluidity of constituent particles, composition and emission processes, which significantly contribute to thermal evolution studies of neutron stars. In Chapter 3 we investigated the question of possible presence of quark matter in the core of a neutron star and reviewed some important factors, such as critical densities for transition from nucleon to quark matter.

In Chapter 4 we developed a model of quark cooling. In the presence of quarks in the core, the main emission process which is responsible for fast cooling, is direct quark URCA process. Our results showed that this direct URCA process is possible in hybrid stars, and with our physical input of TNI 6 EoS of medium stiffness, transition density $\rho_{tr} = 4\rho_0$, and modified HGRR density-dependent superfluid energy gap, we were able to obtain reasonable cooling curves for a neutron star with a quark core.

To conclude, we demonstrated that the present day cooling data can be explained not only by a purely hadronic structure of NS interiors but also by a hybrid one with a pairing pattern, where quarks are paired with the density –dependent gaps of modified HGRR model.

APPENDICES

APPENDIX A

EQUATION OF STATE

There are quite different models for the equation of state under different conditions.

Below Nuclear Density

Below nuclear density, $\rho_0 = 2.8 \times 10^{14}$, the pressure can be expressed as the sum of ion, free electron and free neutron pressures:

$$P = P_{ion} + P_e + P_n, \tag{A.1}$$

Calculate the pressure for P_e and P_n according to the ideal gas laws:

$$P = \frac{1}{3}\int pvn(p)d^3p \tag{A.2}$$

where n(p) is particle number density, and velocity:

$$v = \frac{p}{m} / \sqrt{\left(1 + p/mc^2\right)} \tag{A.3}$$

If the electrons are degenerate, the number density is a function of momentum (Clayton D., 1983):

$$n(p)d^3p = \frac{2}{h^3}\frac{4\pi p^2 dp}{\exp\left[\frac{E-\mu}{k_B T}\right]+1} \tag{A.4}$$

Or

$$n(p)d^3p = \begin{cases} \frac{2}{h^3}4\pi p^2 dp & p \le p_F \\ 0 & p > p_F \end{cases} \tag{A.5}$$

where p_F is Fermi momentum.

Thereby, to calculate the pressure (A.2) we have to figure out the proper conditions for relativistic/non-relativistic and degenerate, partially degenerate and non-degenerate cases.

We know that the criteria for a particle to be relativistic or non-relativistic, degenerate or non-degenerate are following (Clayton D., 1983):

$$\xi_r = \left(\frac{\rho}{7.3 \times 10^6 g/cm^3} \right) \mu_e \qquad \text{(A.6)} \qquad\qquad \xi_d = \left(\frac{\rho}{2.4 \times 10^{-8} g/cm^3} \right) \mu_e T^{3/2} \qquad \text{(A.7)}$$

If $\xi_r \gg 1$, then we have the relativistic case, if $\xi_r \ll 1$, then non-relativistic.

If $\xi_d \gg 1$, then it is degenerate, if $\xi_d \ll 1$, then non-degenerate.

In case of neutron stars the stellar temperature during most of its life is $T \leq 10^9 K$ and thus in the most relativistic regions of the star the matter is also degenerate and in the partially relativistic regions the matter is non-degenerate.

The P_{ion} is just nkT for free gases, because the ions are too heavy to be degenerate and relativistic.

Above Nuclear Density

Inside the core the composition consists of primarily neutrons (95%), protons and electrons (5%). In this region the distance between nucleons is very small due to extremely high densities, and the equation of state can be described by Friedman and Pandharipande (FP) Model (medium), Baym, Pethick and Sutherland (BPS) Model (soft) and Pandharipande and Smith (PS) Model (stiff).

APPENDIX B

COOPER PAIRS

For a system of fermions, if there are attractive interactions between them, fermions can pair and form bosons under certain conditions. These pairs of fermions are called the Cooper Pairs (Baym G., 1974, Lectures On Quantum Mechanics)**.**

Let H be the Hamiltonian of two fermions with the attractive interaction:

$$H = \frac{p_1^2}{2m} + \frac{p_2^2}{2m} + V \tag{B.1}$$

where V is non-positive, because of the attractive nature of the interaction. Let |φ> be the wave function of this two-fermion system. The Shrödinger equation is then:

$$H \mid \varphi\rangle = E \mid \varphi\rangle \tag{B.2}$$

Consider two electrons outside the Fermi surface. Between these two electrons, when their momenta are within a certain range above the Fermi sea, i.e. when their momenta are larger than the Fermi momentum p_f and smaller than p_a, with p_a as a momentum slightly higher than p_f, there will be a weak attractive force between them. This kind of attractive force is caused by the attractive Coulomb force between ions and the two electrons.

For two free electrons, the total wavefunction is:

$$\Psi\left(\vec{r}_1, \vec{r}_2, t\right) = \frac{e^{i\vec{k}_1\vec{r}_1}}{\sqrt{L^3}} e^{\frac{-ik_1 t}{\hbar}} \frac{e^{i\vec{k}_2\vec{r}_2}}{\sqrt{L^3}} e^{\frac{-ik_2 t}{\hbar}} \tag{B.3}$$

with L^3 as the total volume and $k_i=p_i/h$. The wavefunction of these two weakly interacting electrons can be written as a sum of the wavefunctions of two non-interacting electrons:

$$\Psi\left(\vec{r}_1,\vec{r}_2,t\right)=\sum_{\vec{k}_1,\vec{k}_2} a_{\vec{k}_1,\vec{k}_2}\frac{e^{i\vec{k}_1\vec{r}_1}}{\sqrt{L^3}}\frac{e^{i\vec{k}_2\vec{r}_2}}{\sqrt{L^3}}e^{\frac{-iEt}{\hbar}} \qquad \text{(B. 4)}$$

After solving the Shrödinger equation we will find the condition for the ground state energy, and hence the condition for fermions pairing up and forming bosons.

If the temperatures are sufficiently low, i.e. lower than the critical temperature of the boson system, Bose condensation will take place and the system will undergo the transition from the normal state to the superfluid state.

APPENDIX C

VORTEX PINNING

In this section we will introduce the velocity between the superfluid and the crust that can be sustained by vortex pinning (B. Link, 2011).

Vortex pinning fixes the local superfluid velocity in the laboratory frame. As the star spins down, a velocity difference v between the neutron pinned vortices and the neutron superfluid develops. This velocity reaches the critical value v_c at which the *Magnus force*, the hydrodynamic lift force on vortices, would unpin them. The Magnus force per unit length of vortex is:

$$f_{mag} = \rho k v , \tag{C.1}$$

where ρ is the superfluid mass density, k = h/m is the quantum vorticity, where h is Planck constant $h=6.62\times10^{-27}$ cm·g/s and m is twice the neutron mass. Above the critical velocity v_c, the Magnus force will exceed the pinning force and the vortex will get unpinned. If a vortex is bend to intersect nuclei of spacing a, the critical velocity would be given as:

$$\rho k v_c a = F_p , \tag{C.2}$$

where F_p is the characteristic force of the vortex – nucleus potential.

As the vortex possesses large self energy or tension, there is a requirement for the critical velocity when the vortex cannot bend over some certain length l_p:

$$v_c = \frac{F_p}{\rho k a}\left(\frac{a}{l_p}\right) \tag{C.3}$$

Tension lowers the critical velocity by a factor a/l_p. On average, over a length l_p the vortex bends by an amount of δr to intersect one nucleus in a volume $l_p\pi(\delta r)^2$.

The quantities l_p and δr are related by:

$$a^{-3} l_p \pi (\delta r)^2 = 1 \tag{C.4}$$

The energy of the vortex per unit length is:

$$\frac{E_v}{l_p} \cong \frac{1}{2} T_v \frac{(\delta r)^2}{l_p^2} - \frac{E_p}{l_p} \quad , \tag{C.5}$$

where E_p is the interaction energy between a vortex and a single nucleus.

Combining equations (C.4) and (C.5) we get:

$$\frac{l_p}{a} = \left(\frac{3aT_v}{2\pi E_p} \right)^{1/2} \tag{C.6}$$

The vortex tension takes a form of:

$$T_v = \frac{\rho k^2}{4\pi} (0.116 - \ln k_v \xi) \quad , \tag{C.7}$$

where ξ is the radius of the vortex core and k_v is the characteristic bending wavenumber.

At a density of $\rho = 5 \cdot 10^{13}$ g/cm^3 the lattice spacing is a~50fm and the radius of the vortex core is $\xi \sim 10$ fm. For $E_p = 1$ MeV simultaneous solutions of equations (C.6) and (C.7) gives $l_p \sim 9a$.

Combining all the equations the velocity is found to be:

$$v_c = \frac{F_p}{\rho k a}\left(\frac{a}{l_p}\right) = \frac{E_p}{\rho k a \xi}\left(\frac{2E_p}{3aT_v}\right)^{1/2} \tag{C.8}$$

For E_p = 1 MeV and ξ = 10 fm, the critical velocity is $v_c = 4\times10^5$ cm/s.

REFERENCES CITED

Adams W.S., An A-Type of Very Low Luminosity. Publications of the Astronomical Society of the Pacific 26 (155): 198. Retrieved Nov. 7, 2008.

Amundsen L., Ostgarrd E.: Nucl. Phys. A 442, 163, 1985.

Baade W., Zwicky F.: Phys. Rev. 46, 76, 1934.

Bahcall J.N., Wolf R.A.: Phys. Rev. B 140, 1452, 1965.

Baym G., Pethick C., Sutherland P.: Ap. J. 170, 299, 1971.

Baym G., Lectures on Quantum Mechanics, ISBN: 978-0805306675, Pub. Date: 1974

Becker, W., & Pavlov, G. , et al., in The Century of Space Science, 2002.

Becker, W. et al., Astrophysics and Space Science Library, ISBN 9783540769644, Volume 357, 701, 2009.

Blaschke D., Voskresensky D.N., Grigorian H. "Cooling of neutron stars with color cuperconducting quark cores", 2004.

Bohr A., Mottelson B. R., and Pines D. Phys. Rev. 110, 936–938, 1958.

Bowyer S., Byram E.T., Chubb T.A., Friedman H.: Nature 201, 1307, 1964.

Cameron A. G. W: Ap. J. 130, 884, 1959.

Chen H., Baldo M., Burgio G. F., Schulze H.-J., Phys. Rev. D84, 105023, 2011.

Chiu, H.-Y., Ann. Phys. (N.Y.) 26, 364, 1964.

Chiu, H.-Y., Salpeter E.E.: Phys. Rev. Lett. 12, 412, 1964.

Clayton D.D., Principles of Stellar Evolution and Nucleosynthesis, 1983.

Cottam L., Paerels F., Mendez M., Nature 420, 51, 2002.

Drago A., Fiolhais M., Tambini U., arXiv.org > hep-ph > arXiv:hep-ph/9503462, 1995.

Flowers E.G., Ruderman M., Sutherland P.G.: Ap. J. 205, 541, 1976.

Friedman B., Pandharipande V.R.: Ap. J. Nucl. Phys. A 361, 502, 1981.

Gell-Mann M. (1964). "A Schematic Model of Baryons and Mesons". Phys. Lett. 8 (3): 214–215, 1964

Ghosh S. K., Phatak S. C., Phys. Rev. C 52, 2195–2202, 1995.

Giacconi R., Gursky H., Paolini F.R., Rossi B.B: Phys. Rev. Lett. 9, 439, 1962.

Gonzaltz, M. E., Kaspi, V.M., Lyne, A. G., & Pivovaroff, M. J., ApJ, 610, L37, 2004.

Griffiths D. "Introduction to elementary particles", ISBN 006042513X, Pub. date 1987.

Gursky H, Giacconi R, Paolini F.R., Rossi B.B.: Phys. Rev. Lett. 11, 530, 1963.

Halzen F., Martin A., "Quarks and leptons: an introductory course in modern particle physics", Pub. Date 1984, ISBN 0471887412.

Hayakawa S., Prog. Theor. Phys. Suppl., 1964.

Halpern, J. P., Gotthelf, E. V., Camilo, F., Helfand, D. J., & Ransom, S. M., ApJ, 612, 398, 2004.

Hewish A., Bell S. J., Pikington J. D. H., Scott P.F., Collins R.A.: Nature 217, 709, 1968.

Hoffberg M, et al. Phys. Rev. Lett. 24 775, 1970.

Hughes, J. P., Slane, P. O., Park, A., Roming, P. W. A., & Burrows, D. N., ApJ, 591, L109, 2003.

Irvine J.M., "Heavy nuclei, superheavy nuclei, and neutron stars", 1975.

Iwamoto N., Phys. Rev. Lett., 44 (24), 1980.

Kargaltsev, O. Y., Pavlov, G. G., Zavlin, V. E., & Romani, R. W., ApJ, 625, 307, 2005.

Klevansky S.P., Rev. Mod. Phys. 64, 649–708, 1992.

Lattimer J.M., Pethick C.J., Prakash M, Haensel P.: Phys. Rev. Lett. 66, 2701 "Direct URCA process in neutron stars", 1991.

Link B. Instability of Superfluid Flow in the Neutron Star Inner Crust, Mon. not. R. Astron. Soc. 000, 1-8, 2011.

Maieron C., Baldo M., Burgio. G.F., Schulze H.-J., Phys. Rev., D 70, 04310, 2004.

McGowan, K. E., Zane, S., Cropper, M., Kennea, J. A., C´ordova, F. A., Ho, C., Sasseen, T., & Vestrand, W. T., ApJ, 600, 343, 2004.

Meltzer, D. W., and Thorne, K. S., *Ap. J.*, 145, 514, 1966.

Migdal A B Usp. Fiz. Nauk 105 781, 1971.

Motch, C., Zavlin, V. E., & Haberl, F., A&A, 408, 323, 2003.

Nomoto N., Tsuruta S.: Ap. J. 312, 711, 1987.

Oppenheimer J.R., Volkoff G. M.: Phys. Rev. 55, 374, 1939.

Page D., Lattimer J.M., Prakash M., Steiner A.W.: Ap. J. Suppl. Series 155, 623, 2004.

Pandharipande V.R., Pines D., Smith R.A.: Ap. J. 208, 550, 1976.
Pavlov, G. G., Zavlin, V. E., Aschenbach, B., Trumper, J., & Sanwal, D., ApJ, 531, L53, 2000.

Pavlov G.G., Zavlin V.E., Sanwal D., Burwitz V., Garmire G.P. ApJ., 554, L189, 2001.

Pavlov, G. G., Zavlin, V. E., & Sanwal, D., in Proc. 270th WE-Heraeus Seminar on Neutron Stars, Pulsars and Supernova Remnants, MPE Rep. 278, 273, 2002.

Pons, J. A.,Walter, F. M., Lattimer, J. M., Prakash, M., Neuhauser, R., & An, P, ApJ, 564, 981, 2002.

Qin L., PhD Thesis at MSU, 1995.

Rodrigues H., Duarte S.B., Oliveira J. C. T., Nuclear Physics B (Proc. Suppl.) 199, 333–336, 2010.

Shapiro S.L., Teukolsky S.A., Black Holes, White Dwarfs, and Neutron Stars, New-York: Wiley-Interscience, 1983.

Slane, P., in Young Neutron Stars and Their Environments, ed. F. Camilo et al. (San Francisco, CA: ASP), 185, 2004.

Steiner, A. W., & Reddy, S., submitted, arXiv:0804.0593S, 2008.

Takatsuka T.: Prog. Theor. Phys. 48, 1517, 1972.

Takatsuka T., Tamagaki R., Prog. Theor. Phys. 64, 2270, 1980.

Takatsuka T., Tamagaki R., Prog. Theor. Phys. 67, 1649, 1982.

Tsuruta S.: Neutron Star Models. PhD Thesis, Columbia University, New York. 1964.

Tsuruta S., Cameron A. G. W.: Canad. J. Phys. 44, 1863, 1966.

Tsuruta S., in: M.P. Ulmer (Ed.) 13th Texas Symp. Rel. Astrophys., World Scientific, Singapore, 1987.

Tsuruta S., Phys. Reports, V. 292, 1, "Thermal properties and detectability of neutron stars". 1998.

Tsuruta S., Sadino J., Kobelski A., Teter M.A., Liebmann A. C., Takatsuka T., Nomoto K., Umeda H.l, Astrophys. Journal, 691:621-632, 2009.

Tsuruta S.: On the Present and Future of Pulsar Astronomy, ASSL, Springer Lectures Series, ed. W. Becker (AIP), pp. 289 – 318, 2010.

Umeda H., Shibazaki N., Nomoto K., Tsuruta S.: Ap. J. 408, 186 (1993).

Umeda H., Nomoto K., Tsuruta S., Muto T., Tatsumi T.: Ap. J. 431, 309 (1994).

Umeda H., Tsuruta S., Nomoto K.: Ap. J. 433, 256 (1995).

Weisskopf, M. C., O'Dell, S. L., Paerels, F., Elsner, R. F., Becker, W., Tennant, A. F., & Swartz, D. A., ApJ, 601, 1050, 2004.

Wheeler J.A., Harrison B.K, Wakano M.: In: La Structure et l'evolution de l'univers, ed by T. Stoops (Brussels 1958); E.E. Salpeter: Ap. J. 134, 669, 1961.

Yakovlev D.G., Levenfish K. P., Shibanov Yu. A., Physics-Uspekhi 42, 73, 1999.

Zavlin V.E., Trumper J., Pavlov G.G., ApJ, 525, 959, 1999.

Zavlin, V. E., & Pavlov, G. G, in Proc. XMM-Newton, 75, EPIC Consotium Memorie della Societa Astronomica Italiana, G58, 2004.

Zweig G., "An SU (3) Model for Strong Interaction Symmetry and its Breaking", CERN Report No.8182/TH.401, 1964.